LETTER

doi:10.1038/nature12283

Unusual architecture of the p7 channel from hepatitis C virus

Bo OuYang[1,2,3], Shiqi Xie[4], Marcelo J. Berardi[1], Xinhao Zhao[4], Jyoti Dev[1], Wenjing Yu[4], Bing Sun[4,5] & James J. Chou[1,2,3]

The hepatitis C virus (HCV) has developed a small membrane protein, p7, which remarkably can self-assemble into a large channel complex that selectively conducts cations[1–4]. We wanted to examine the structural solution that the viroporin adopts in order to achieve selective cation conduction, because p7 has no homology with any of the known prokaryotic or eukaryotic channel proteins. The activity of p7 can be inhibited by amantadine and rimantadine[2,5], which are potent blockers of the influenza M2 channel[6] and licensed drugs against influenza infections[7]. The adamantane derivatives have been used in HCV clinical trials[8], but large variation in drug efficacy among the various HCV genotypes has been difficult to explain without detailed molecular structures. Here we determine the structures of this HCV viroporin as well as its drug-binding site using the latest nuclear magnetic resonance (NMR) technologies. The structure exhibits an unusual mode of hexameric assembly, where the individual p7 monomers, *i*, not only interact with their immediate neighbours, but also reach farther to associate with the *i*+2 and *i*+3 monomers, forming a sophisticated, funnel-like architecture. The structure also points to a mechanism of cation selection: an asparagine/histidine ring that constricts the narrow end of the funnel serves as a broad cation selectivity filter, whereas an arginine/lysine ring that defines the wide end of the funnel may selectively allow cation diffusion into the channel. Our functional investigation using whole-cell channel recording shows that these residues are critical for channel activity. NMR measurements of the channel–drug complex revealed six equivalent hydrophobic pockets between the peripheral and pore-forming helices to which amantadine or rimantadine binds, and compound binding specifically to this position may allosterically inhibit cation conduction by preventing the channel from opening. Our data provide a molecular explanation for p7-mediated cation conductance and its inhibition by adamantane derivatives.

Many viruses have developed integral membrane proteins to transport ions and other molecules across the membrane barrier to aid various steps of viral entry and maturation[9,10]. These membrane structures, known as viroporins, usually adopt minimalist architectures that are significantly different from those of bacterial or eukaryotic ion channels. Therefore, understanding the structural basis of how viroporins function broadens our knowledge of channels and transporters while generating new opportunities for therapeutic intervention.

The viroporin formed by the HCV p7 protein has been sought after as a potential anti-HCV drug target[5,11]. p7 is a 63-residue membrane protein that oligomerizes to form ion channels with cation selectivity, for Ca^{2+} over K^+ and Na^+ (refs 2, 3, 12, 13), and a more recent study has also reported p7-mediated H^+ intracellular conductance[14]. The p7 channel is required for viral replication[15]; it has been shown to facilitate efficient assembly and release of infectious virions[16,17], although the precise mechanism of these functions remains unclear. The channel activity can be inhibited by adamantane and long alkyl chain iminosugar derivatives and hexamethylene amiloride *in vitro*, with varying reported efficacies[2,3,12,13]. In addition to ion conduction, p7 has been shown to specifically interact with the non-structural HCV protein NS2, indicating that its channel activity could be regulated[18,19].

There is not yet a detailed structure of the p7 channel, although a number of NMR studies showed that the p7 monomer has three helical segments: two in the amino-terminal half of the sequence and one near the carboxy terminus[12,20]. A single-particle electron microscopy (EM) study obtained a 16 Å resolution electron density map of the p7 oligomer using the random conical tilting approach[4]. The map shows that the p7 channel is a 42-kDa hexamer and adopts a flower-like shape that does not resemble any of the known ion channel structures in the database.

It is not known how the small p7 polypeptide assembles into what appears to be a complex channel structure, and whether the viroporin has adopted novel structural elements for cation selectivity and channel gating. Amantadine or rimantadine blocks the influenza M2 channel by binding to the small pore formed by four transmembrane helices[21–23], but the pore of the p7 hexamer is expected to be much bigger and it is thus unclear how these small molecules would fit. We sought to address these questions by determining detailed structures of the p7 hexamer and its drug-binding site.

We systematically tested p7 amino acid sequences from various HCV genotypes and found that the sequence from genotype 5a (EUH1480 strain) generated samples that were sufficiently soluble for structure determination (Supplementary Fig. 1). This p7 construct, designated here as p7(5a), could be efficiently reconstituted in dodecylphosphocholine (DPC) micelles at near physiological pH and generated high-quality NMR spectra (Supplementary Fig. 2). Negative-stain EM of the DPC-reconstituted p7(5a) in NMR buffer showed hexameric, flower-shaped particles that are similar to those in the electron micrographs of the p7 (JFH-1 strain, genotype 2a) hexamer in dihexanoyl-phosphatidyl-choline (DHPC) micelles used earlier for single-particle reconstruction[4] (Supplementary Fig. 3). Moreover, isothermal titration calorimetry and NMR chemical shift perturbation analyses of p7(5a)–rimantadine interaction showed that the drug binds specifically to the reconstituted protein with a binding constant (K_d) from 50 to 100 μM at 3 mM detergent concentration (Supplementary Figs 4 and 5). The above results together indicate that the p7(5a) polypeptides reconstituted in DPC micelles form structurally relevant hexamers.

Structure determination of the p7(5a) hexamer by NMR used an approach taken earlier for oligomeric membrane proteins[24–26], which involves: (1) determination of local structures of the monomers; and (2) assembly of the oligomer with intermonomer distance restraints and orientation constraints. The NMR-derived restraints define an ensemble of structures with backbone root mean squared deviation (r.m.s.d.) of 0.74 Å (Fig. 1a). Each monomer consists of an N-terminal helix (H1) from residues 5–16, a middle helical segment (H2), with a

[1]Department of Biological Chemistry and Molecular Pharmacology, Harvard Medical School, Boston, Massachusetts 02115, USA. [2]State Key Laboratory of Molecular Biology, Shanghai Institute of Biochemistry and Cell Biology, Chinese Academy of Sciences, Shanghai 200031, China. [3]National Center for Protein Science, Shanghai Institute of Biochemistry and Cell Biology, Chinese Academy of Sciences, Shanghai 200031, China. [4]Molecular Virus Unit, Key Laboratory of Molecular Virology and Immunology, Institut Pasteur of Shanghai, Shanghai Institutes for Biological Sciences, Chinese Academy of Sciences, Shanghai 200025, China. [5]State Key Laboratory of Cell Biology, Shanghai Institute of Biochemistry and Cell Biology, Chinese Academy of Sciences, Shanghai 200031, China.

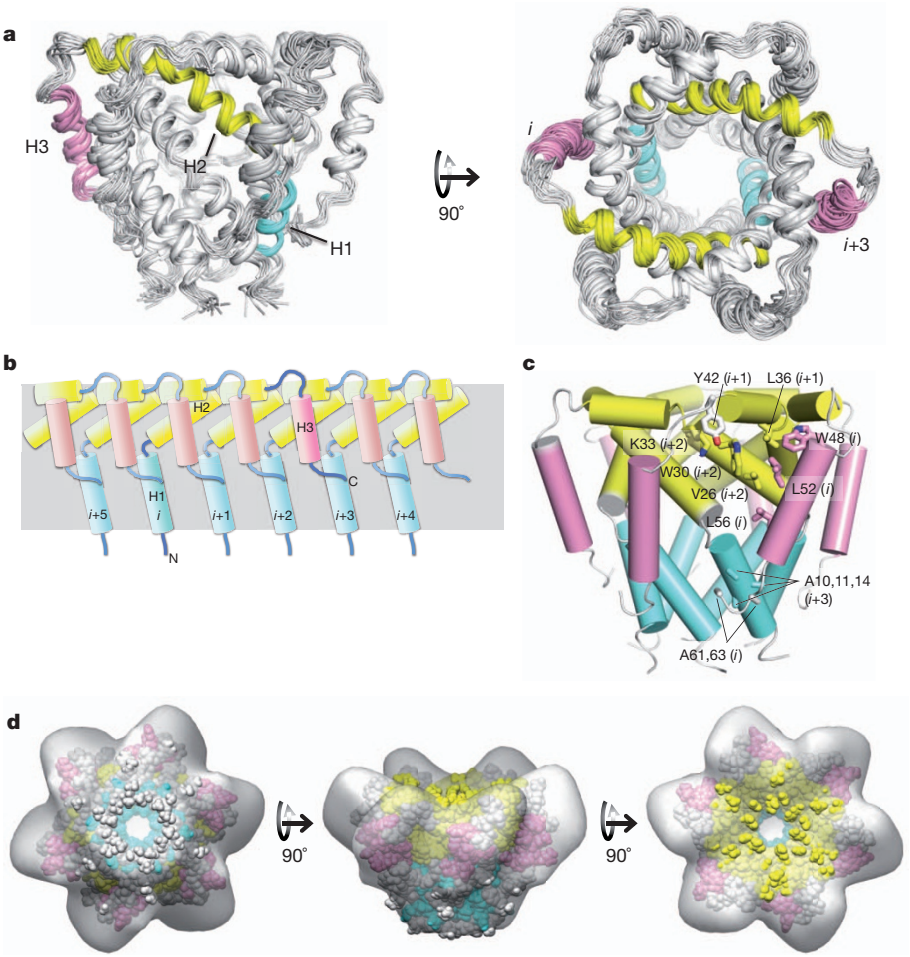

Figure 1 | NMR structure of the p7(5a) hexamer and its comparison to the EM map. **a**, Ensemble of 15 low-energy structures calculated using NMR restraints summarized in Supplementary Table 1. **b**, Two-dimensional drawing illustrating the intermonomer interactions among the H1 (blue), H2 (yellow) and H3 (pink) helical segments that are responsible for the hexameric assembly. **c**, Three-dimensional cartoon representation describing the global arrangement of helical segments and amino acids that seem to have a role in the packing of H3 against H1 and H2. **d**, Fitting the lowest-energy structure from the ensemble to the 16 Å EM map (EM database ID 1661)[4]. The fitting correlation is 0.94 as calculated with the program Chimera.

kink at Gly 34, from residues 20–41, and a C-terminal helix (H3) from residues 48–58. These secondary structures are consistent with earlier NMR studies of p7 monomers in DHPC detergent and organic solvent[12,20]. There are no intramonomer contacts (Fig. 1a). The monomers are intertwined to form a tightly packed channel, where H1 and H2 form the channel interior and H3 is lipid-facing and packs against H2 of the $i+2$ and H1 of the $i+3$ monomer (Fig. 1a, b). The intermonomer association between H3 and H2 appears to be stabilized by interaction involving conserved residues such as Trp 30, Tyr 42 and Leu 52, and the contacts between H3 and H1 are mostly between the alanine-rich region of H1 (residues 10–15) and Ala 61 and Ala 63 of H3 (Fig. 1c). The overall structure of the p7(5a) hexamer has a flower-like shape that agrees with the EM map (EM database ID 1661), fitting to the map with a correlation coefficient of 0.94 (Fig. 1d).

The channel cavity has a funnel profile that resembles a champagne flute and is largely hydrophilic (Fig. 2a). The H2 helices form the wide cylindrical region (internal diameter (ID) ~12 Å) by packing with each other at large angles (angle between adjacent helices approximately −47°), and the H1 helices assemble at smaller packing angles (approximately −34°) to form the narrow conical region of the funnel (smallest ID at 6.8 Å). Residues 17–19 constitute the flexible joint between H1 and H2; their NMR resonances are significantly broader than other regions of the protein, indicating the presence of conformational exchange.

The channel architecture described above represents a novel topology and exemplifies how HCV has optimized the short p7 polypeptide to achieve a rather complex channel structure. We next addressed what elements are involved in cation conduction and gating. An in-depth examination of the channel interior found two strongly conserved polar residues with salient structural features (Fig. 2b). One is Asn 9, which forms a ring of carboxamide that constricts the conical region of the channel (Fig. 2c). Residue 9 is asparagine in all strains except in genotype 2 viruses, where it is substituted with histidine. Both asparagines and histidines have affinity for monovalent and divalent cations. We propose that the Asn 9 ring serves as a broad selectivity filter that dehydrates cations, allowing them to pass the hydrophobic ring formed by Ile 6. The Ile 6 ring defines the narrowest point of the channel and probably serves as a hydrophobic gate. Another feature is the Arg 35 ring that defines the wider, C-terminal end of the channel (Fig. 2b). Placement of a positively charged ring on the other end of the pore was incomprehensible to us initially because it can repel cations. But the recent structure of an Orai Ca^{2+} channel also revealed a stretch of basic residues in the ion-conducting pore[27]. We propose that one role of Arg 35 is to bind and obstruct anions at the pore entrance while allowing cations to diffuse into the pore. In this model, cation conduction is unidirectional from the C- to N-terminal end of the channel.

To test the above hypotheses, we established an assay that uses the two-electrode voltage-clamp technique to record p7-mediated current in *Xenopus* oocytes (see Methods). Owing to the poor stability of oocytes that overexpress p7(5a), p7 (JFH-1 strain, genotype 2a) was used instead for these experiments. As expected because of the proposed role of residue 9 in selectively dehydrating cations, replacing His 9 of p7(2a) with alanine caused a ~70% reduction in channel conductance at +80 mV (Fig. 2d). The proposed role of Arg 35 indicates that placing negatively charged residues at the channel entrance would bind cations and hinder their diffusion into the pore, and indeed the Arg35Asp mutation also reduced conductance by ~70% (Fig. 2d).

We next investigated the mechanism of amantadine binding to the p7 channel using proteins that are ^{15}N-labelled and deuterated so that nuclear Overhauser enhancement (NOE) between the protein backbone

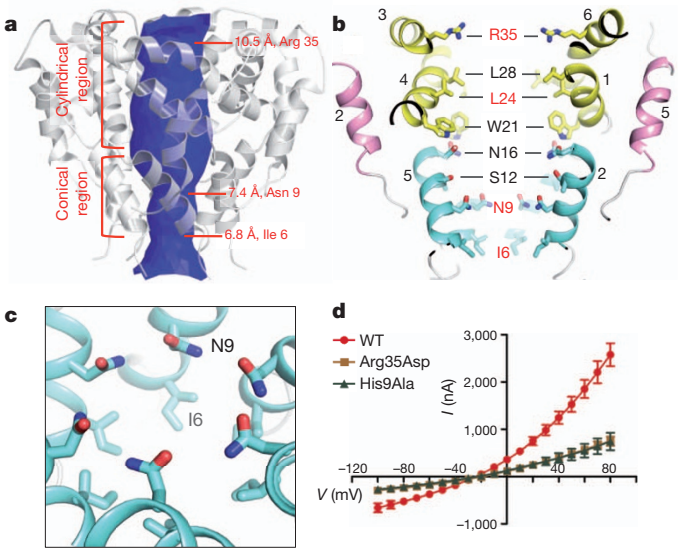

Figure 2 | The pore properties of the p7(5a) channel. **a**, The pore surface calculated using the program HOLE, showing the shape and constrictions of the pore. **b**, Sectional view of the channel showing the pore-lining residues with residues in red being strongly conserved. The numbers next to the helical segments represent the monomers to which the helices belong. Colour scheme as in Fig. 1. **c**, A close-up view of the rings formed by Asn 9 and Ile 6 that constrict the N-terminal end of the channel. **d**, The current–voltage relationships of wild-type (WT) p7(2a) and the His9Ala and Arg35Asp mutants. Each data point is the mean ± s.e.m. (standard error of mean) calculated over measurements from six different oocytes ($n = 6$).

amide protons and drug protons could be measured unambiguously. At 10 mM amantadine (not corrected for drug partitioning to detergent micelles), the ^{15}N-edited nuclear Overhauser enhancement spectroscopy (NOESY) spectrum showed NOE crosspeaks between the adamantane protons and the amide protons of Val 26, Leu 55, Leu 56 and Arg 57 (Fig. 3a). We then identified contacts between the drug and protein side chains using protein that is (^{1}H/^{13}C)-labelled at the methyl positions of alanines, valines and leucines but is otherwise deuterated. In this case, the ^{13}C-edited NOESY showed several methyl-drug NOEs (Fig. 3b).

These NOEs were used to dock amantadine into the structure determined in the absence of drug. In doing so, we emphasize that the relevance of the p7–amantadine complex is confined to only the drug-binding region because we do not know how and to what degree does drug binding alter the global conformation of the channel. The relatively poor stability of the protein–drug complex at the current stage of our study precludes full-scale structure determination. Nonetheless the available NMR data show that the drug adamantane binds to six equivalent hydrophobic pockets between the pore-forming and peripheral helices (Fig. 3c). The pocket consists of Leu 52, Val 53 and Leu 56 from H3, and Phe 20, Val 25 and Val 26 from H2. The amantadine amino group on average points to the channel lumen. The same NOESY spectrum as above recorded using a sample with 5 mM rimantadine indicates that rimantadine binds to the same pocket with the methyl and amino groups pointing to the lumen (Supplementary Fig. 6).

The binding site is overall consistent with a mutational study showing that mutations in residues 50–55 significantly reduce drug sensitivity of the channel[28]. It is also consistent with a Leu20Phe mutation in genotype 1b virus originally identified in clinical trials that confers amantadine resistance[8,29]. In the p7(5a) structure, residue 20 is an integral part of the drug pocket and is in direct contact with the drug adamantane. Therefore, replacing Leu 20 in p7(1b) with phenylalanine is expected to reduce hydrophobic interaction with the drug. Elucidation of previous functional data in the context of the structure suggests that the binding site shown in Fig. 3c is relevant to drug inhibition and that interactions between the drug adamantane and protein hydrophobic residues are critical for inhibition. Variations in the hydrophobicity of the binding pocket among the p7 variants (Supplementary Fig. 7) thus explain the large differences in drug efficacies observed between different HCV genotypes.

We have learnt from KcsA and other channels that a gated ion channel generally adopts two essential features: pore elements that provide ion selectivity, and a gating mechanism that can transiently

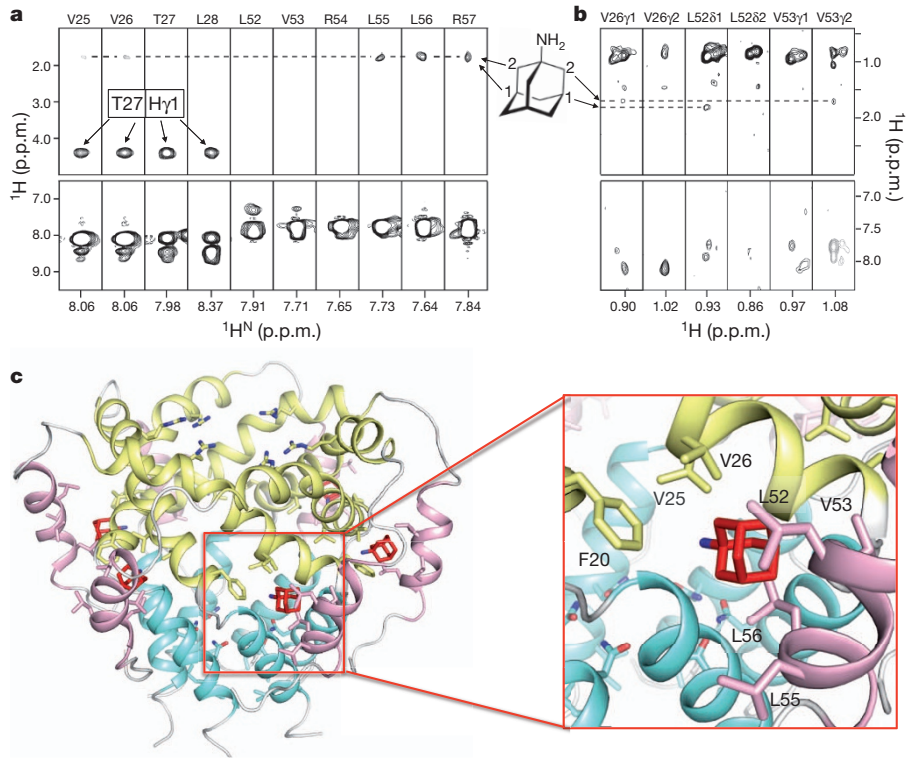

Figure 3 | NMR characterization of the amantadine binding site. **a**, Representative strips from the three-dimensional ^{15}N-edited NOESY-TROSY (transverse relaxation optimized spectroscopy) spectrum (300 ms NOE mixing time) recorded using a sample containing ^{15}N-, ^{2}H-labelled p7(5a) and 10 mM amantadine, showing amantadine NOEs to the backbone amide protons of Val 26, Leu 55, Leu 56 and Arg 57. **b**, Representative strips from the three-dimensional diagonal-suppressed ^{13}C-edited NOESY-HSQC spectrum recorded using a sample that is ^{1}H-, ^{13}C-labelled at the methyl positions of alanines, valines and leucines but is otherwise deuterated, showing drug NOEs to the side-chain methyl protons of Val 26, Leu 52 and Val 53. The spectra in **a** and **b** were recorded at ^{1}H frequency of 900 MHz. **c**, Amantadine docked into the p7(5a) hexamer using restraints from NOEs in **a** and **b** (left) and a close-up view of amantadine in the binding pocket (right). Colour scheme as in Fig. 1.

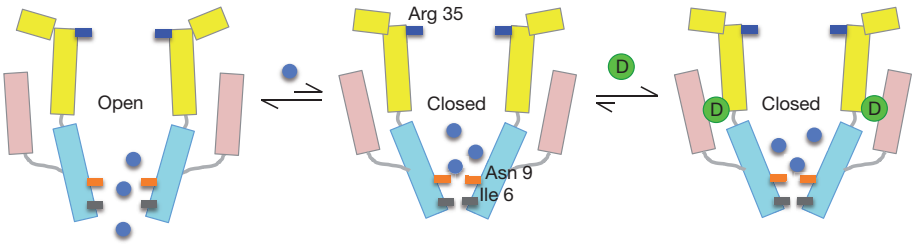

Figure 4 | A model for amantadine or rimantadine inhibition of the p7 channel. The two-dimensional cartoon drawing mimics the sectional view of the p7 channel in Fig. 2b. The channel undergoes conformational switching between the closed and the open states but favours the open state in the presence of cations (blue circles). Binding of amantadine or rimantadine (green circles, labelled with 'D' for drug) favours the closed state by restricting movements of the three helical segments that may be required for channel opening.

open the channel to allow ion permeation. By virtue of being a funnel, the p7 structure indicates that the tip of the funnel represented by the Ile 6 and Asn 9 rings is the key region for channel gating (Fig. 4). The role of the Asn 9 ring is to provide ion selectivity by recruiting and dehydrating cations near the funnel exit, whereas the Ile 6 ring is a hydrophobic constriction that would prevent water from freely passing through. Channel activation may involve reorientation of the H1 helices that widens the funnel tip, analogous to the dynamic C-terminal helix of KcsA[30], and such structural rearrangement can be afforded by the flexible hinge between H1 and H2, the intervening loop between H2 and H3, and the C-terminal tail that 'latches' onto H1. We thus propose that binding of adamantane derivatives inhibit channel activity by restricting the structural rearrangement. Our NMR titration data (Supplementary Fig. 5c) are consistent with this proposal, which shows that in the absence of rimantadine, the Ile 6 methyl resonance is split into an intense and weak peak, possibly corresponding to the open and closed state, respectively, and that increasing the drug concentration shifts the equilibrium that make the weak peak stronger. Although rigorous testing of the model is needed, the preliminary observation suggests the existence of multiple states of the p7 channel.

METHODS SUMMARY

The p7 sequence from HCV genotype 5a was mutated at five unconserved positions to improve protein stability and to facilitate NMR analyses (see details in Supplementary Fig. 1). The protein was expressed as a fusion to His 9–trpLE that formed inclusion bodies, and purified and reconstituted in DPC as previously described[23,25]. A typical NMR sample contains 0.8 mM protein (monomer concentration), 200 mM DPC and 25 mM MES (pH 6.5).

For structure determination, the secondary structures of the p7(5a) monomers in the hexamer were first determined using standard NOE experiments. We then used a mixed sample in which 50% of the monomers are (^{15}N/^{2}H)-labelled and 50% ^{13}C-labelled to measure exclusively NOEs between the ^{15}N-attached protons of one subunit and the ^{13}C-attached protons of the neighbouring subunits. This experiment provided key intermonomer NOEs between adjacent H1 and H2 helices for assembling the central cavity of the hexamer (Supplementary Fig. 8a). H3 was positioned based on orientation restraints from residual dipolar couplings (RDCs) and its intermonomer NOEs to H1 and H2 (Supplementary Fig. 8b, c). Structure calculation statistics are given in Supplementary Table 1. Protein–drug contacts were identified using (^{15}N/^{2}H)-labelled protein so that NOEs between protein backbone amide protons and drug protons could be identified unambiguously. Additionally, NOEs between the drug and protein side-chain methyl groups were measured with a diagonal-suppressed carbon NOESY using ALV labelled protein (see Methods).

Functional p7 mutants were analysed using the standard protocol for two-electrode voltage-clamp of *Xenopus* oocytes. After expressing the p7(2a) variants in oocytes, we recorded p7 currents across the oocyte plasma membrane at room temperature (~22 °C). For quantitative comparison of currents between the p7 variants, the protein expression levels in oocytes were examined using confocal microscopy.

Full Methods and any associated references are available in the online version of the paper.

Received 17 January; accepted 22 April 2013.
Published online 5 June 2013.

1. Moradpour, D., Penin, F. & Rice, C. M. Replication of hepatitis C virus. *Nature Rev. Microbiol.* **5,** 453–463 (2007).
2. Griffin, S. D. *et al.* The p7 protein of hepatitis C virus forms an ion channel that is blocked by the antiviral drug, amantadine. *FEBS Lett.* **535,** 34–38 (2003).
3. Pavlovic, D. *et al.* The hepatitis C virus p7 protein forms an ion channel that is inhibited by long-alkyl-chain iminosugar derivatives. *Proc. Natl Acad. Sci. USA* **100,** 6104–6108 (2003).
4. Luik, P. *et al.* The 3-dimensional structure of a hepatitis C virus p7 ion channel by electron microscopy. *Proc. Natl Acad. Sci. USA* **106,** 12712–12716 (2009).
5. Griffin, S. *et al.* Genotype-dependent sensitivity of hepatitis C virus to inhibitors of the p7 ion channel. *Hepatology* **48,** 1779–1790 (2008).
6. Wang, C., Takeuchi, K., Pinto, L. H. & Lamb, R. A. Ion channel activity of influenza A virus M2 protein: characterization of the amantadine block. *J. Virol.* **67,** 5585–5594 (1993).
7. Davies, W. L. *et al.* Antiviral activity of 1-sdamantanamine (amantadine). *Science* **144,** 862–863 (1964).
8. Mihm, U. *et al.* Amino acid variations in hepatitis C virus p7 and sensitivity to antiviral combination therapy with amantadine in chronic hepatitis C. *Antivir. Ther.* **11,** 507–519 (2006).
9. Fischer, W. B. & Sansom, M. S. Viral ion channels: structure and function. *Biochim. Biophys. Acta* **1561,** 27–45 (2002).
10. Nieva, J. L., Madan, V. & Carrasco, L. Viroporins: structure and biological functions. *Nature Rev. Microbiol.* **10,** 563–574 (2012).
11. Steinmann, E. *et al.* Antiviral effects of amantadine and iminosugar derivatives against hepatitis C virus. *Hepatology* **46,** 330–338 (2007).
12. Montserret, R. *et al.* NMR structure and ion channel activity of the p7 protein from hepatitis C virus. *J. Biol. Chem.* **285,** 31446–31461 (2010).
13. Premkumar, A., Wilson, L., Ewart, G. D. & Gage, P. W. Cation-selective ion channels formed by p7 of hepatitis C virus are blocked by hexamethylene amiloride. *FEBS Lett.* **557,** 99–103 (2004).
14. Wozniak, A. L. *et al.* Intracellular proton conductance of the hepatitis C virus p7 protein and its contribution to infectious virus production. *PLoS Pathog.* **6,** e1001087 (2010).
15. Sakai, A. *et al.* The p7 polypeptide of hepatitis C virus is critical for infectivity and contains functionally important genotype-specific sequences. *Proc. Natl Acad. Sci. USA* **100,** 11646–11651 (2003).
16. Jones, C. T., Murray, C. L., Eastman, D. K., Tassello, J. & Rice, C. M. Hepatitis C virus p7 and NS2 proteins are essential for production of infectious virus. *J. Virol.* **81,** 8374–8383 (2007).
17. Steinmann, E. *et al.* Hepatitis C virus p7 protein is crucial for assembly and release of infectious virions. *PLoS Pathog.* **3,** e103 (2007).
18. Popescu, C. I. *et al.* NS2 protein of hepatitis C virus interacts with structural and non-structural proteins towards virus assembly. *PLoS Pathog.* **7,** e1001278 (2011).
19. Vieyres, G. *et al.* Subcellular localization and function of an epitope-tagged p7 viroporin in hepatitis C virus-producing cells. *J. Virol.* **87,** 1664–1678 (2013).
20. Cook, G. A. & Opella, S. J. Secondary structure, dynamics, and architecture of the p7 membrane protein from hepatitis C virus by NMR spectroscopy. *Biochim. Biophys. Acta* **1808,** 1448–1453 (2011).
21. Stouffer, A. L. *et al.* Structural basis for the function and inhibition of an influenza virus proton channel. *Nature* **451,** 596–599 (2008).
22. Cady, S. D. *et al.* Structure of the amantadine binding site of influenza M2 proton channels in lipid bilayers. *Nature* **463,** 689–692 (2010).
23. Pielak, R. M., Oxenoid, K. & Chou, J. J. Structural investigation of rimantadine inhibition of the AM2–BM2 chimera channel of influenza viruses. *Structure* **19,** 1655–1663 (2011).
24. Oxenoid, K. & Chou, J. J. The structure of phospholamban pentamer reveals a channel-like architecture in membranes. *Proc. Natl Acad. Sci. USA* **102,** 10870–10875 (2005).
25. Schnell, J. R. & Chou, J. J. Structure and mechanism of the M2 proton channel of influenza A virus. *Nature* **451,** 591–595 (2008).
26. Van Horn, W. D. *et al.* Solution nuclear magnetic resonance structure of membrane-integral diacylglycerol kinase. *Science* **324,** 1726–1729 (2009).
27. Hou, X., Pedi, L., Diver, M. M. & Long, S. B. Crystal structure of the calcium release-activated calcium channel Orai. *Science* **338,** 1308–1313 (2012).
28. StGelais, C. *et al.* Determinants of hepatitis C virus p7 ion channel function and drug sensitivity identified *in vitro*. *J. Virol.* **83,** 7970–7981 (2009).
29. Foster, T. L. *et al.* Resistance mutations define specific antiviral effects for inhibitors of the hepatitis C virus p7 ion channel. *Hepatology* **54,** 79–90 (2011).
30. Cuello, L. G., Jogini, V., Cortes, D. M. & Perozo, E. Structural mechanism of C-type inactivation in K^+ channels. *Nature* **466,** 203–208 (2010).

Supplementary Information is available in the online version of the paper.

Acknowledgements We thank R. Sounier for helping with making specific methyl-labelled protein, S. Brueschweiler for helping with ITC measurements, G. Bellot, J. Min and W. Shih for providing DNA nanotube liquid crystal, and K. Oxenoid for discussion. This work was supported by the National Key Project of 973 (2013CB530504) and National Science and Technology Major Project (2012ZX10002-007-003) (to B.S.) and NIH grant GM094608 (to J.J.C.).

Author Contributions B.O. and J.J.C. conceived the study; B.O. prepared samples; M.J.B. performed EM analysis; J.D. and B.O. performed NMR titration; B.O. and J.J.C. collected and analysed NMR data and determined the structure; S.X., X.Z., W.Y. and B.S. designed and performed functional experiments; J.J.C. wrote the paper and all authors contributed to the editing of the manuscript.

Author Information The structure is deposited in the Protein Data Bank under the accession number 2M6X. Reprints and permissions information is available at www.nature.com/reprints. The authors declare no competing financial interests. Readers are welcome to comment on the online version of the paper. Correspondence and requests for materials should be addressed to J.J.C. (chou@cmcd.hms.harvard.edu) or B.S. (bsun@sibs.ac.cn).

METHODS

Sample preparation. The amino acid sequence of p7 from genotype 5a was slightly modified to allow for efficient reconstitution and protein sample stability. In this sequence, Thr 1 is replaced with Gly, Ala 12 is replaced with Ser, and the three cysteines at positions 2, 27 and 44 are replaced with Ala, Thr and Ser, respectively (Supplementary Fig. 1). The p7(5a) construct was cloned, expressed and purified as previously described[23,25]. Briefly, the protein was expressed as a fusion to His9–trpLE that formed inclusion bodies. The peptide was released from the fusion protein by CNBr digestion and subsequently separated on a Proto-18C column by reverse-phase chromatography (more details given in Supplementary Methods). The lyophilized peptide was then dissolved in 6 M guanidine and DPC and refolded by dialysis against the NMR buffer. A typical NMR sample contains 0.8 mM protein (monomer concentration), 200 mM DPC and 25 mM MES (pH 6.5).

Assignment of NMR resonances. All NMR experiments were conducted at 30 °C on Bruker spectrometers equipped with cryogenic probes. Sequence-specific assignment of backbone chemical shifts was accomplished using three pairs of triple resonance experiments, recorded using a $^{15}N/^{13}C/^{2}H$-labelled sample. The triple resonance experiments were relaxation optimized (TROSY)[31], including HNCA, HN(CO)CA, HNCACB, HN(CO)CACB, HN(CA)CO and HNCO[32]. Protein side-chain aliphatic and aromatic resonances were assigned using a combination of NOESYs including ^{15}N-edited NOESY-TROSY (60 ms NOE mixing time, τ_{NOE}) and ^{13}C-edited NOESY-HSQCs ($\tau_{NOE} = 100$ ms). Specific stereo assignment of the methyl groups of valines and leucines were obtained from a constant-time ^{1}H-^{13}C HSQC spectrum recorded using a 15% ^{13}C-labelled sample[33].

Assignment of local NOEs for determining the secondary structures. The same ^{15}N-edited NOESY-TROSY and ^{13}C-edited NOESY-HSQC above with short τ_{NOE} were used to assign local NOEs. Combining the NOE restraints with chemical shifts, we could very precisely define the helical and loop regions of the individual monomers.

Measurement of residual dipolar coupling (RDC) constants. The backbone ^{1}H-^{15}N RDCs were measured using a modified approach[34] of the strain-induced alignment in a gel method[35,36]. In this experiment the p7(5a) channel in DPC micelles was soaked into a cylindrically shaped polyacrylamide gel (4.5%), initially of 6 mm diameter, which was subsequently radially compressed to fit within the 4.2-mm inner diameter of an open-ended NMR tube. The ^{1}H-^{15}N RDCs were obtained from $^{1}J_{NH}/2$ and $(^{1}J_{NH} + {}^{1}D_{NH})/2$, which were measured by interleaving a regular gradient-enhanced HSQC and a gradient-selected TROSY[37]. The largest ^{1}H-^{15}N RDC measured is 33.5 Hz.

Assignment of intermonomer NOEs. Intermonomer NOEs between protein backbone amide and side-chain methyl protons was assigned using a sample that was reconstituted with a 1:1 mixture of ^{15}N-, ^{2}H-labelled p7(5a) peptide and ^{13}C-labelled peptide. Recording a ^{15}N-edited NOESY-TROSY ($\tau_{NOE} = 300$ ms) on a 900 MHz spectrometer with this sample allowed exclusive detection of NOE crosspeaks between the ^{15}N-attached protons of one monomer and the ^{13}C-attached protons of other monomers. The intermonomer NOEs between the neighbouring H1 helices and neighbouring H2 helices effectively defined the central cavity formed by these helices. The initial structural solution of the pore assembly then allowed us to assign complementary and self-consistent intermonomer NOEs between the aliphatic and aromatic protons in a pair of ^{15}N-edited NOESY-TROSY and ^{13}C-edited NOESY-HSQC recorded using a ^{15}N-, ^{13}C-labelled sample. These spectra were recorded with τ_{NOE} of 120 ms and 150 ms, respectively.

The packing of H1 and H2 helices between the adjacent monomers and RDC-derived orientation constraints together positioned the H3 helix of monomer *i* to be in contact with H2 of the *i*+2 and H1 of the *i*+3 monomers, and this conformation was confirmed by the unambiguous amide-methyl NOEs between H3 and H1/H2. The conformation as defined by the intermonomer NOEs was subjected to numerous rounds of self-consistency test with the NOE crosspeaks in the ^{13}C-edited NOESY-HSQC spectrum to ensure that all NOEs are consistent with the structure. The overall distribution of intermonomer NOEs is illustrated in Supplementary Fig. 7.

Assignment of NOEs between protein and drug. We prepared a sample containing ^{15}N-, ^{2}H-labelled p7(5a), 10 mM amantadine (or 5 mM rimantadine), and perdeuterated DPC. The sample was used to record a ^{15}N-edited NOESY-TROSY ($\tau_{NOE} = 300$ ms) on a 900 MHz spectrometer. This experiment allowed exclusive detection of NOEs between the exchangeable amide protons and the drug protons. For assigning NOEs between the protein side-chain methyl protons and the drug protons, we prepared the ALV-labelled protein that is ^{1}H-, ^{13}C-labelled at the methyl positions of alanines, valines and leucines but is otherwise deuterated. The NOEs were measured using a ^{13}C-edited NOESY with diagonal suppression, that is, interleaving two experiments: one with NOE mixing (300 ms) of the H_z magnetization (NOE crosspeaks) and the other with mixing of the H_zC_z magnetization (no NOE crosspeaks)[38]. Subtracting the two spectra mostly cancelled the strong methyl diagonal peaks (~0.8 p.p.m.) and thereby unveiled the weak methyl-drug NOEs at ~1.7 p.p.m.

Structure calculation of the p7(5a) hexamer. Structures were calculated using the program XPLOR-NIH[39]. The monomer structures (mainly the secondary structures) were first calculated using intramonomer NOE-derived distance restraints, backbone dihedral restraints derived from chemical shifts using the TALOS program[40], and RDC restraints. A total of 10 monomer structures were calculated using a standard simulated annealing (SA) protocol. Six copies of the lowest-energy monomer structure were used to construct an initial model of the hexamer using intermonomer NOE restraints collected from the mixed-labelled sample for the H1 and H2 helical segments. For each intermonomer restraint between two adjacent monomers, six identical distance restraints were assigned respectively to all pairs of neighbouring monomers to satisfy the condition of C6 rotational symmetry (as indicated by the EM data). The assembled hexamer was then subjected to refinement against RDCs to accurately orient the three helical segments. Finally, using the SA protocol, the hexamer was refined against the complete set of NOE restraints (including intramonomer and intermonomer distance restraints), dihedral restraints and RDC restraints. A total of 60 hexamer structures were calculated and 15 low-energy structures were selected as the structural ensemble. Ramachandran plot statistics for the structure ensemble, calculated using PROCHECK[41], are as follows: most favoured (96.6%), additionally allowed (2.8%), generously allowed (0.6%) and disallowed (0.0%).

Whole-cell channel recording assay for p7. The cRNA of p7(2a) variants was synthesized and injected into *Xenopus laevis* oocytes at ~15 ng per oocyte. After about 16–30 h of expression, healthy oocytes were collected and subjected to channel recording using the two-electrode voltage-clamp technique[42]. The oocytes were first bathed in standard ORi solution (90 mM NaCl, 2 mM KCl, 2 mM $CaCl_2$ and 5 mM MOPS, pH 7.4) before being impaled with two microelectrodes. For recording p7-mediated current, we used a voltage-clamp protocol consisting of rectangular voltage steps from −100 to +80 mV in 10-mV increments, applied from a holding voltage of −60 mV. Expression levels of the p7 variants in oocytes were examined by confocal microscopy using haemagglutinin-tagged p7. More experimental details are described in Supplementary Methods.

31. Pervushin, K., Riek, R., Wider, G. & Wuthrich, K. Attenuated T2 relaxation by mutual cancellation of dipole-dipole coupling and chemical shift anisotropy indicates an avenue to NMR structures of very large biological macromolecules in solution. *Proc. Natl Acad. Sci. USA* **94,** 12366–12371 (1997).
32. Kay, L. E., Torchia, D. A. & Bax, A. Backbone dynamics of proteins as studied by 15N inverse detected heteronuclear NMR spectroscopy: application to staphylococcal nuclease. *Biochemistry* **28,** 8972–8979 (1989).
33. Szyperski, T., Neri, D., Leiting, B., Otting, G. & Wuthrich, K. Support of 1H NMR assignments in proteins by biosynthetically directed fractional 13C-labeling. *J. Biomol. NMR* **2,** 323–334 (1992).
34. Chou, J. J., Gaemers, S., Howder, B., Louis, J. M. & Bax, A. A simple apparatus for generating stretched polyacrylamide gels, yielding uniform alignment of proteins and detergent micelles. *J. Biomol. NMR* **21,** 377–382 (2001).
35. Sass, H. J., Musco, G., Stahl, S. J., Wingfield, P. T. & Grzesiek, S. Solution NMR of proteins within polyacrylamide gels: Diffusional properties and residual alignment by mechanical stress or embedding of oriented purple membranes. *J. Biomol. NMR* **18,** 303–309 (2000).
36. Tycko, R., Blanco, F. J. & Ishii, Y. Alignment of biopolymers in strained gels: A new way to create detectable dipole-dipole couplings in high-resolution biomolecular NMR. *J. Am. Chem. Soc.* **122,** 9340–9341 (2000).
37. Weigelt, J. Single scan, sensitivity- and gradient-enhanced TROSY for multidimensional NMR experiments. *J. Am. Chem. Soc.* **120,** 10778–10779 (1998).
38. Wu, J., Fan, J. S., Pascal, S. M. & Yang, D. General method for suppression of diagonal peaks in heteronuclear-edited NOESY spectroscopy. *J. Am. Chem. Soc.* **126,** 15018–15019 (2004).
39. Schwieters, C. D., Kuszewski, J., Tjandra, N. & Clore, G. M. The Xplor-NIH NMR molecular structure determination package. *J. Magn. Reson.* **160,** 66–74 (2002).
40. Cornilescu, G., Delaglio, F. & Bax, A. Protein backbone angle restraints from searching a database for chemical shift and sequence homology. *J. Biomol. NMR* **13,** 289–302 (1999).
41. Laskowski, R. A., MacArthur, M. W., Moss, D. S. & Thornton, J. W. PROCHECK: a program to check the stereochemical quality of protein structures. *J. Appl. Cryst.* **26,** 283–291 (1993).
42. Plugge, B. *et al.* A potassium channel protein encoded by chlorella virus PBCV-1. *Science* **287,** 1641–1644 (2000).

doi:10.1038/nature12283

Supplementary Methods

Protein expression and purification

The p7(5a) protein was expressed in E. Coli BL21 (DE3) cells as a fusion to His9-trpLE in the pMM-LR6 vector (gift from S.C. Blacklow, Harvard Medical School, Boston). Transformed BL21(DE3) cells were inoculated in M9 minimal medium and grown at 37°C to OD600 ~ 0.7 and cooled to 25°C for overnight induction with 150 mM IPTG. Inclusion bodies were extracted with buffer containing 6 M guanidine HCl, 50 mM Tris (pH 8.0), 200 mM NaCl, 1% Triton X-100. The cleared lysate was bound to a Ni^{2+} affinity column (Sigma) and washed with the same buffer described above. The His9-trpLE-p7 fusion protein was then eluted from the Ni^{2+} column with 6 M guanidine HCl, 50 mM Tris (pH 8.0), 200 mM NaCl, and 400 mM imidazole at room temperature. The eluted protein was precipitated by dialysis against water, and the precipitants were then digested with CNBr in 70% formic acid (1 hr, 0.2 g/ml) to release the p7(5a) peptide from trpLE. The cleaved products were dialyzed against water, lyophilized, and loaded onto a C18 column (Proto) in 100% formic acid. The column was first washed with Buffer A (40% acetonitrile, 0.1% trifluoroacetic acid (TFA)), and then the peptides were separated using a gradient of 0–60% Buffer B (60% acetonitrile, 0.1% TFA) (**Supplementary Fig. 9**). The overall yield is roughly 5 mg/L. NMR samples were prepared by dissolving 1–2 mg of lyophilized p7 peptide in 6 M guanidine and DPC and refolded by dialysis against the NMR buffer.

Rimantadine titration experiment for p7(5a) oligormer

The major challenge of measuring dissociation constant (K_d) for a hydrophobic drug such as rimantadine in detergent solution is the strong partitioning of drug to free micelles, which effectively reduces the drug concentration available to protein. We first measured binding of rimantadine to p7(5a) by Isothermal Titration Calorimetry (ITC). The advantage of ITC is that we can use lower protein and detergent concentrations than what are required for NMR experiments, thus more meaningful estimation of the drug concentration. The protein samples used for ITC are essentially a diluted version of the NMR sample, which consists of 25 mM MES (pH 6.5), 3 mM DPC, and 20 μM p7 (monomer). We first observed the typical binding saturation profile for p7(5a) (**Supplementary Fig. 4a**). We then tested the effect of a F20L mutation on rimantadine binding. In p7 (strain BK; genotype 1b), residue 20 is a leucine and the L20F mutation was identified originally in clinical trials to confer amantadine or

rimantadine resistance[1,2]. Our structural data in **Fig. 3** suggest that the L20F mutation would significantly reduce hydrophobic interaction between p7(1b) and the drug. Conversely, it is expected that the F20L mutation in p7(5a) should increase rimantadine binding, and the ITC data for the F20L mutant indeed shows this effect (**Supplementary Fig. 4b**). This result further validates the NMR-derived amantadine or rimantadine binding site reported in this paper. Because there are six such sites in the hexamer structure, we used stoichiometry of one drug to one p7 monomer to fit the ITC data and found K_d for rimantadine binding to the p7(5a) wildtype (WT) and the F20L mutant to be 63.6 and 13.2 μM, respectively.

We also performed detailed NMR titration experiment using a ($^{15}N/^{13}C$)-labeled sample with 80 mM DPC and 0.25 mM p7(5a) (monomer concentration), which was optimized for the lowest detergent/protein ratio where high resolution NMR spectroscopy was feasible. Two-dimensional ^{1}H-^{15}N TROSY-HSQC and methyl HSQC were recorded at rimantadine concentrations of 0, 1, 2, 4, and 8 mM (**Supplementary Fig. 5**). The chemical shift changes clearly followed a binding curve but did not saturate even at 8 mM. The large discrepancy in binding saturation with the ITC experiment above is due to the very different detergent concentrations used between the two experiments. In principle, because neither the protein nor rimantadine are water soluble, they reside almost completely in the detergent phase, and thus their effective concentrations need to be scaled by (total volume / detergent volume), or V_{tot}/V_{det}. Furthermore, if the drug partitions preferentially to a particular region of the detergent micelles, e.g., rimantadine partitions between the phosphocholine headgroup and the acyl chain[3], the estimation of K_d is even much more complicated.

We nevertheless conducted another NMR titration experiment using a sample with protein and detergent concentrations very similar to those used in the ITC experiments: 38 μM p7 (monomer) and 3 mM DPC. In this sample, the protein is ALV-labeled – ^{1}H-, ^{13}C-labeled at the methyl positions of alanines, valines and leucines but is otherwise deuterated. This isotope labeling scheme removes the one-bond ^{13}C-^{13}C *J* coupling to permit the use of the more sensitive regular carbon evolution (as opposed to the constant-time carbon evolution) and minimizes dipolar relaxation by deuteration. The above sample optimization, combined with the use of cryogenic NMR probe, enabled acquisition of ^{1}H-^{13}C HSQC spectra at micromolar protein concentration. As anticipated of the use of much lower detergent concentration, rimantadine titration led to a much faster saturation of chemical shift changes (see specific movements of the resolved peaks for the methyl groups of Val25 and Val53 in **Supplementary Fig. 5c**). Fitting of NMR titration data as in the ITC experiment yielded apparent K_d of

96.5 and 46.9 μM for Val25 γ2 and Val53 γ1 methyl groups, respectively. These values are in good agreement with the ITC experiment (see **Supplementary Fig. 4a**).

Negative-stain EM of the reconstituted p7(5a) oligomer

We examined channel formation of p7(5a) in DPC micelles by negative stain EM. We applied 4 μL of a 200 nM p7 protein solution in 3 mM DPC, 25 mM MES, pH 6.5 to a hydrophilic glow discharged copper grid coated with a thin carbon film. The sample was blotted after soaking for 20 seconds and washed 3 times with water and once with stain (0.8% Uranyl formate pH 5.0). Stain was applied for one minute, and excess stain solution was removed by vacuum aspiration. A total of 30 images were recorded on a Philips Tecnai-12 electron microscope equipped with a LaB6 filament and a 4K × 4K Gatan CCD detector. The microscope was operated using low dose procedures at a magnification of 100,000 ×, de-focus to ~0.6 μm, with an acceleration voltage of 80 kV to maximize contrast. Images were binned by 2 × 2 pixels, for a final 1.8 Å /pixel resolution.

Image processing, particle selection and image alignment and classification were performed using the EMAN2 program suit[4] (**Supplementary Fig. 3a-d**). We selected a total of 817 raw particle images using four circularly averaged internal templates. Templates were handpicked from the images and centered in an area of 10 × 10 nm. Particles sizes varied from 4 to 7 nm due to the presence of multiple orientations as well as the resolution-limiting effect of the stain grain used in our study. Raw particle images were CTF corrected and subjected to 20 cycles of alignment and classification into 15 output classes. Representative class averages corresponding to 'top' and 'side' projections were compared to the projection images obtained using the previously reported 16 Å EM 3D reconstitution map of the p7(2a) hexamer in DHPC micelles and the 16 Å map calculated from our NMR structure. Projections with the highest normalized cross-correlation values are compared side by side in **Supplementary Fig. 3e**.

Docking amantadine into the p7(5a) channel using protein-drug NOE restraints

We used a total of eight protein-amantadine distance restraints, derived from the eight NOEs shown in **Fig. 3a&b**, to dock the amantadine into the p7(5a) channel structure. In this experiment, the hexamer structure was used as a starting model, which was refined using the XPLOR-NIH protocol described in METHODS against protein-drug NOE restraints and structural restraints acquired for the drug-free

channel. In doing so, we assumed that amantadine binding does not significantly alter the protein conformation. Although this assumption may not be correct, i.e., drug binding could alter the global conformation, we believe that the local structural details of the amantadine binding site as provided by the calculated structures are reasonably accurate because the protein-drug NOE restraints did not conflict with any of the protein structural restraints.

Whole-cell channel recording assay

p7 cRNA synthesis and microinjection p7 cDNA for various mutants were synthesized by recursive PCR and amplified by primers with restriction sites for BglII (5' end) and SalI (3' end) enzymes[5]. The amplified fragments were then cut by the two enzymes and cloned into expression vector pNWP (kindly provided by Fei Jian) with a SP6 promoter. The plasmid was linearized by NotI digestion and transcribed *in vitro* to cRNA following the manual of the mMESSAGE mMACHINE high-yield capped RNA transcription SP6 Kit (Ambion)[6]. For protein expression in oocytes, 15 ng of cRNA were injected into one oocyte with Micro 4^{TM} Microsyringe Pump Controller (World Precision Instrument).

Oocyte preparation and voltage clamping Oocytes were obtained from *Xenopus Laevis* by surgery as described previously[6,7]. Briefly, pieces of ovary from female frogs were dissected and then defolliculated by treatment with collagenase (Sigma). Oocytes injected with cRNA were incubated at 18 °C in standard ND96 solution (96 mM NaCl, 2 mM KCl, 1.8 mM $CaCl_2$, 1.0 mM $MgCl_2$, 5 mM HEPES and 2.5 mM sodium pyruvate, adjusted to pH 7.4 with NaOH) for 16~30 hours before current recording. Higher amount of cRNA injection or longer incubation time caused death of oocytes. Whole-oocyte currents were recorded using the standard two-electrode voltage clamp technique (OC-725C, Warner Instrument Corp.). The oocytes were bathed in a chamber of ~1.4 ml ORi solution (90 mM NaCl, 2 mM KCl, 2 mM $CaCl_2$, and 5 mM MOPS, pH 7.4) at room temperature (~22 °C) and impaled with microelectrodes filled with 3 M KCl (tip resistance of 1-5 MΩ). Currents were generated by applying the rectangular voltage protocol from −100 to +80 mV in 10 mV increments with a holding voltage of −60 mV, and analyzed by the pCLAMP 10.0 software package (Axon Instruments).

Current measurements and validation of the functional assay p7 from two genotypes, p7(5a) from strain EUH1480 and p7(2a) from strain JFH-1, were initially used for current recording. Water injected oocytes were used as a negative control (NC). Overexpression of p7(5a) unfortunately caused damage

to oocyte membrane that led to high frequency of oocyte death, whereas oocytes expressing p7(2a) are generally in good condition and produced stable currents. We thus used p7(2a) and its mutants for performing systematic measurements of p7-mediated currents.

We first found that oocytes injected with p7(2a) cRNA exhibited large, outward current that is distinct from the small, non-specific currents from the NC oocytes (**Supplementary Fig. 10a**). Moreover, p7(2a)-mediated current in the ooctye is sensitive to Na^+/K^+ composition in the ORi solution (**Supplementary Fig. 10b**), consistent with earlier reports that the p7 channel is permeable to cations such as Na^+ and K^+[8,9].

We then injected cRNA of the N-terminal HA-tagged p7(2a) into the oocytes and examined protein expression and localization by confocal microscopy. The oocytes expressing HA-tagged p7(2a) showed currents similar to those expressing p7(2a). After current recording, the oocytes that expressed HA-tagged p7(2a) were fixed with 5% paraformaldehyde and immuno-labeled with anti-HA (1:100 dilution) antibody (Sigma). The immuno-labeled oocytes were then monitored using a TCS SP2 confocal microscope (Leica Microsystems). The fluorescent images clearly show p7(2a) expression and localization in the cell membrane (**Supplementary Fig. 11**).

Supplementary Table 1 NMR and refinement statistics for the p7(5a) hexamer

	p7(5a) hexamer
NMR distance and dihedral constraints	
Distance constraints	
Intramonomer	224 x 6
Short-range ($\|i - j\| \leq 4$)	224 x 6
Long-range ($\|i - j\| \geq 5$)	0
Intermonomer	24 x 6
Total dihedral angle restraints	78 x 6
ϕ (TALOS)	39 x 6
ψ (TALOS)	39 x 6
Total RDCs	49 x 6
Backbone NH	49 x 6
Structure statistics [a]	
Violations (mean ± s.d.)	
Distance constraints (Å)	0.065 ± 0.003
Dihedral angle constraints (°)	3.033 ± 0.064
RDC constraints (Hz)	2.721 ± 0.023
Deviations from idealized geometry	
Bond lengths (Å)	0.004 ± 0.000
Bond angles (°)	0.697 ± 0.006
Impropers (°)	0.685 ± 0.008
Average pairwise r.m.s. deviation (Å) [b]	
Heavy	1.180
Backbone	0.739

[a] Statistics are calculated and averaged over an ensemble of the 15 lowest energy structures.

[b] The precision of the atomic coordinates is defined as the average r.m.s. difference between the 15 final structures and their mean coordinates. The calculation only includes the structured regions of the protein: residues 5-16, 20-41, and 48-58.

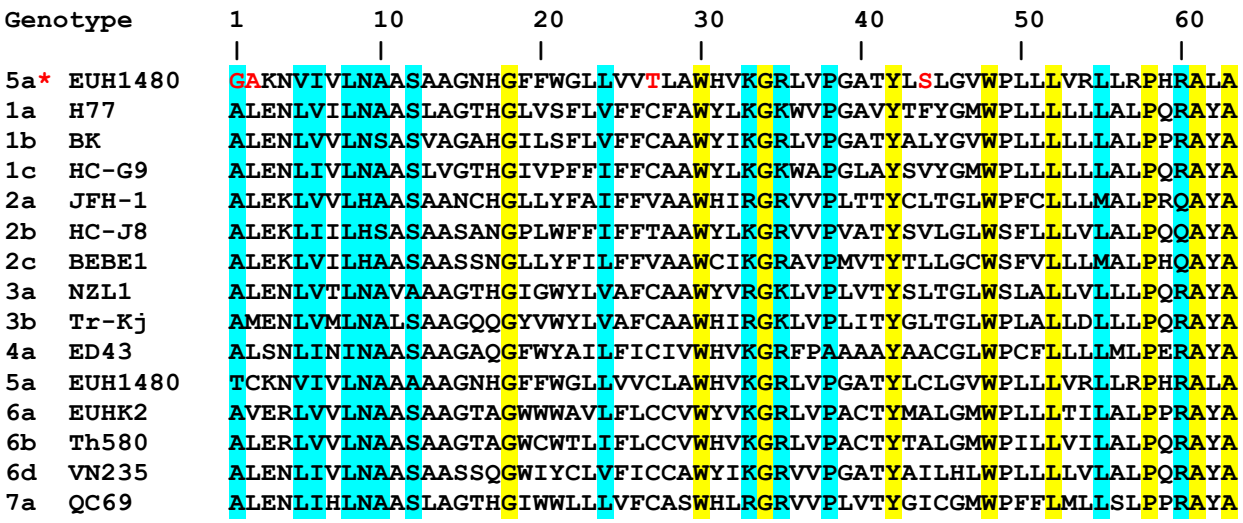

Supplementary Figure 1. Alignment of multiple p7 sequences from the known HCV genotypes shows substantial sequence variability. Residue positions shaded in yellow and in cyan correspond to identity and conservative substitution, respectively. The first sequence, labeled 5a*, is the modified 5a sequence used for our structural studies. In this sequence, Thr1 is replaced with Gly, Ala12 is replaced with Ser, and the three cysteines at positions 2, 27, and 44 are replaced with Ala, Thr, and Ser, respectively. None of the five residue positions is conserved.

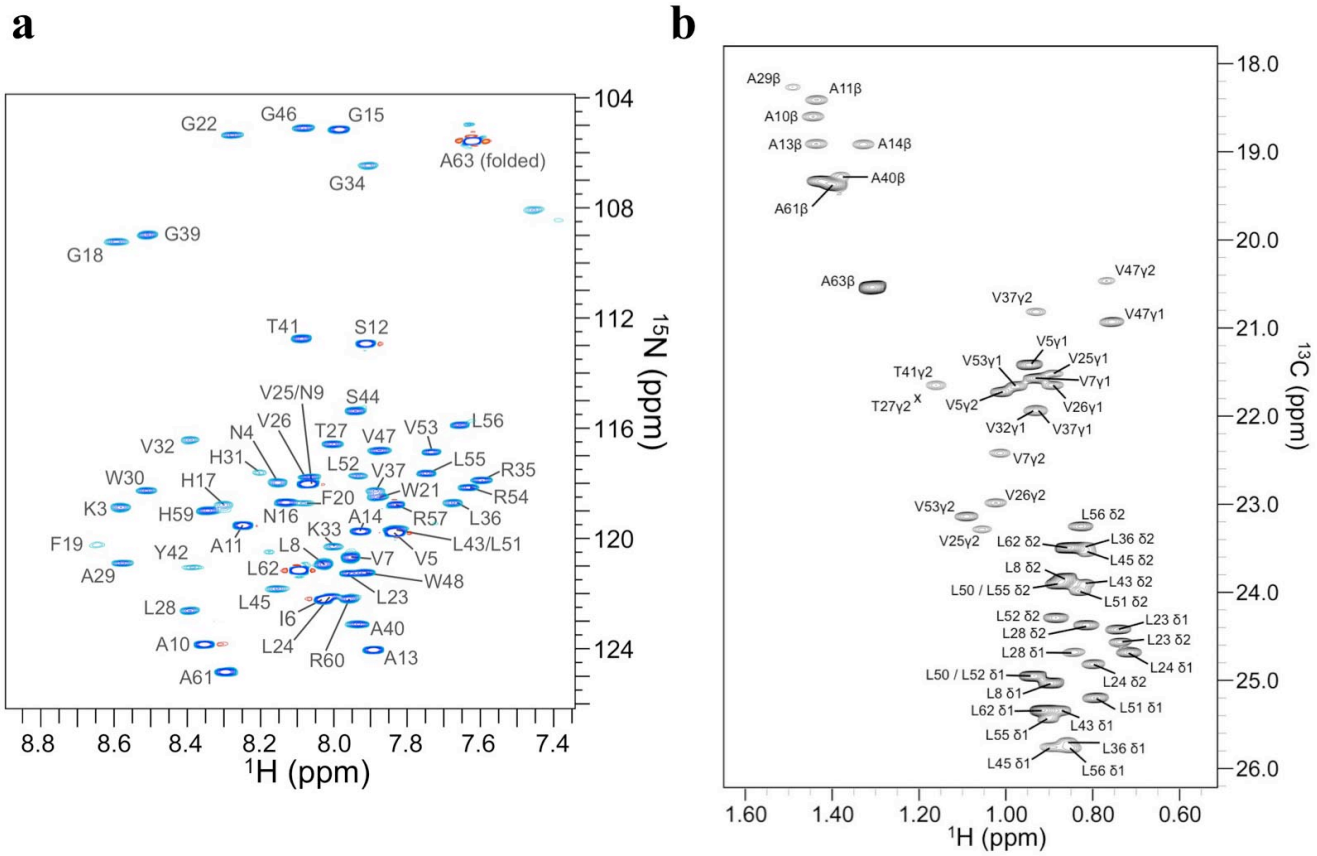

Supplementary Figure 2. NMR spectra of p7(5a) hexamer reconstituted in DPC micelles at pH 6.5.

a, Two-dimensional ^{1}H-^{15}N TROSY-HSQC spectrum of ^{15}N-, ^{13}C-, ^{2}H-labeled p7(5a) hexamer reconstituted in DPC micelles at pH 6.5 (recorded at ^{1}H frequency of 900 MHz). The labels are residue-specific assignments of the amide resonances.

b, Completely assigned NMR spectrum of the methyl groups of the p7^{5a} hexamer reconstituted in deuterated DPC micelles at pH 6.5 and 30 °C. The ^{1}H-^{13}C HMQC (non-constant-time ^{13}C evolution) experiment was performed at ^{1}H frequency of 900 MHz using a protein sample that is (^{1}H, ^{13}C)-labeled at the methyl positions of alanines, valines and leucines but is otherwise deuterated and ^{12}C-labeled.

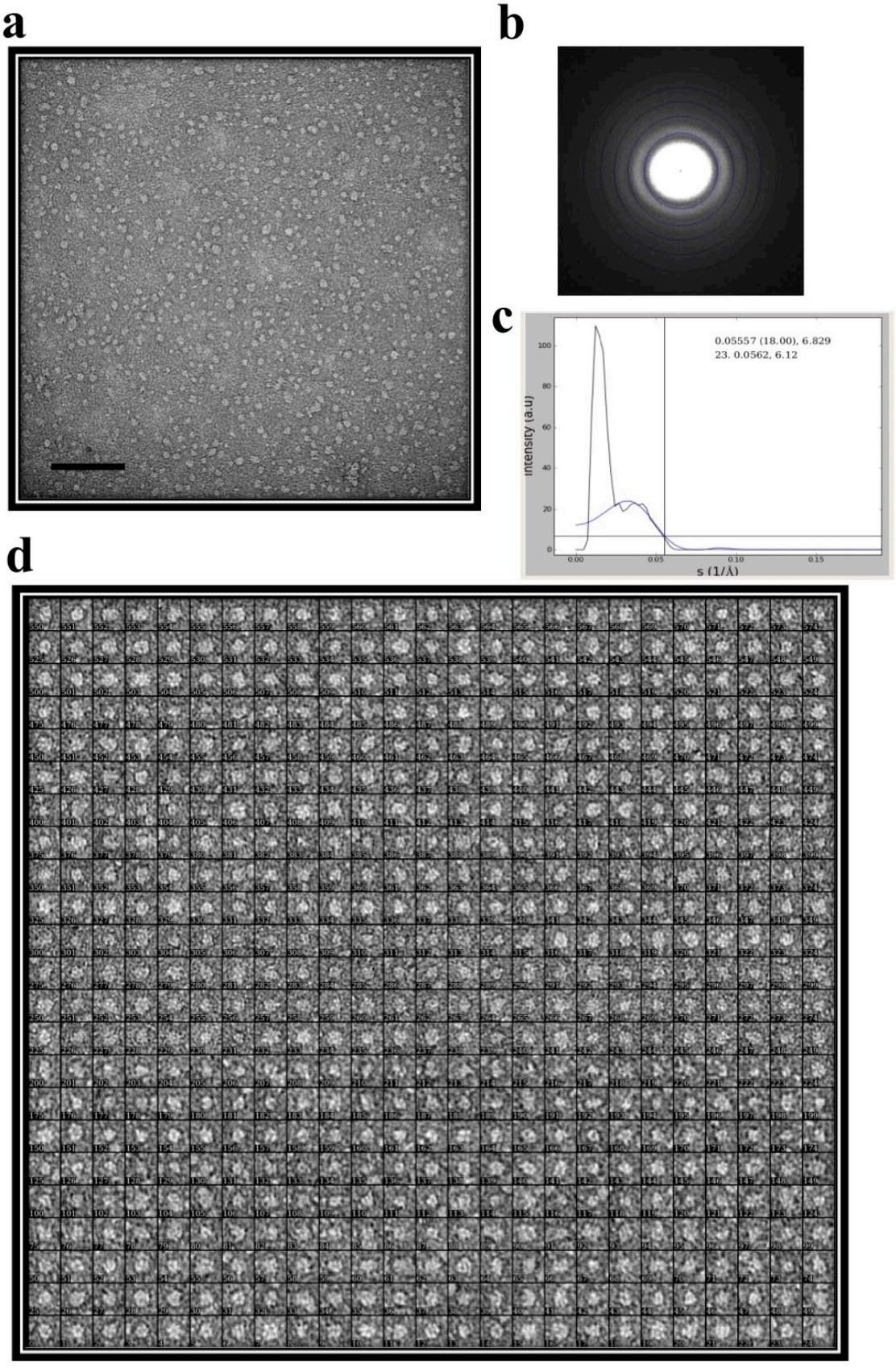
a
b
c
0.05557 (18.00), 6.829
23. 0.0562, 6.12
Intensity (a.u)
s (1/Å)
d

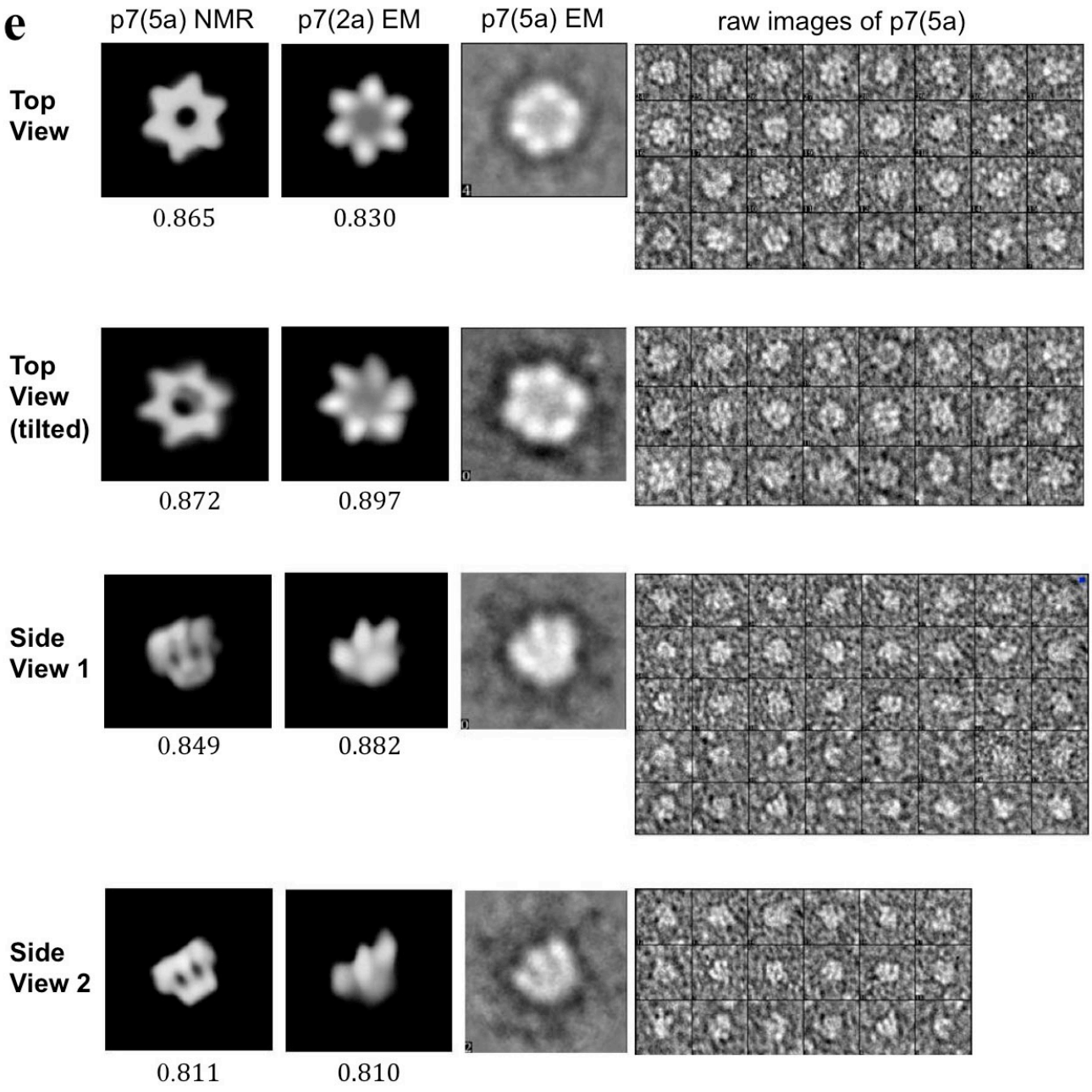

Supplementary Figure 3. Negative-stain EM analysis of the p7(5a) NMR sample

a, Typical image of the p7(5a) oligomers from our NMR sample negatively stained with uranyl formate at low magnification. Bar corresponds to 50 nm in length.

b, 2D-FFT of the image with rings marking the nodes used to estimate the contrast transfer function.

c, Reciprocal plot of intensities, showing that our images contain information to at least 18 Å (cross hair estimation).

d, Representative subset of raw images (~500) that were automatically selected using four handpicked templates.

e, Representative class averages corresponding to 'top' and 'side' projections (column 3) are compared to the projection images of the 16 Å map calculated from our NMR structure (column 1) and to the projection images of the previously reported 16 Å EM map of p7(2a) (JFH-1 strain) in DHPC micelles[10]. The projection images that fit the best to the class averages in column 3 are shown in this figure and the corresponding normalized cross-correlation values are labeled below the images. The raw particle image set for each of the class average is present in column 4.

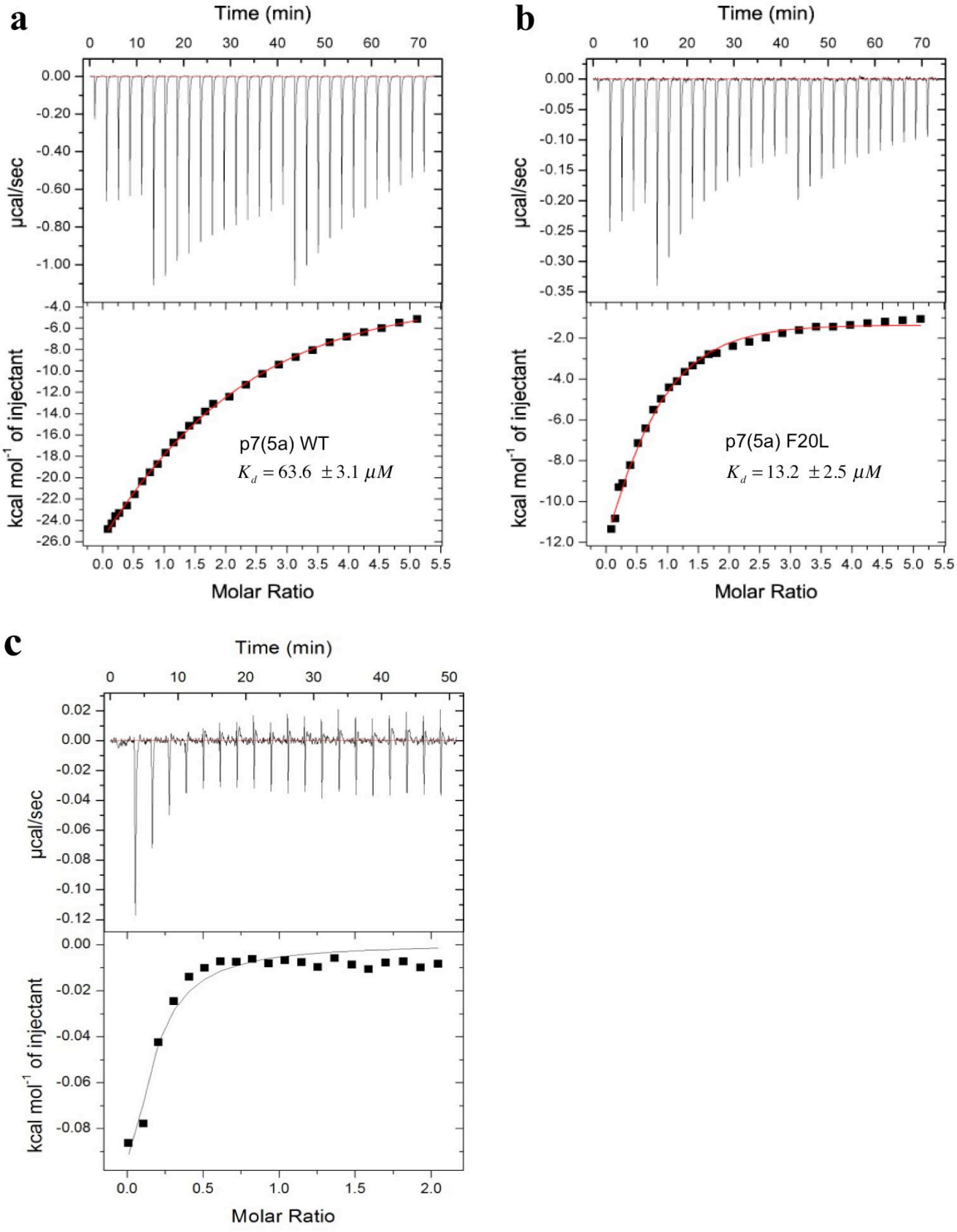
a
Time (min)
µcal/sec
kcal mol-1 of injectant
p7(5a) WT
$K_d = 63.6 \pm 3.1\ \mu M$
Molar Ratio
b
Time (min)
µcal/sec
kcal mol-1 of injectant
p7(5a) F20L
$K_d = 13.2 \pm 2.5\ \mu M$
Molar Ratio
c
Time (min)
µcal/sec
kcal mol-1 of injectant
Molar Ratio

Supplementary Figure 4. Isothermal titration calorimetry analysis of rimantadine binding to the p7(5a) hexamer.

a, The p7(5a) construct used for NMR measurements. **b,** The p7(5a) construct used for NMR measurements with single mutation F20L. The protein samples used for ITC are diluted version of the NMR sample, which consists of 25 mM MES (pH 6.5), 3 mM DPC, and 20 μM p7 (monomer). The drug stock solution contains 20 mM rimantadine in 25 mM MES (pH 6.5) and 3 mM DPC. The titration protocol involved injecting 0.5 μL drug stock solution to 250 μL protein solution for the first 4 additions, 1 μL for the middle 12 additions, and 2 μL for the last 12 additions. The top graphs in (**a**) and (**b**) show raw data in terms of μcal/second plotted against time in minutes. The bottom graphs show normalized integration data in terms of kcal/mole of injectant plotted against molar ratio. Data fitting involved adjusting the effective drug concentration to reach 1:1 p7 monomer:drug stoichiometry. The two horizontal axes are linked, so that the integrated area for each peak appears directly below the corresponding peak in the raw data. Experiments were performed at 30 °C using Microcal ITC200 (GE Healthcare).

c, Titrating rimantadine into empty DPC micelles. Twenty injections of ligand solution were added to detergent solution in the ITC cell. Ligand solution contains: 25 mM MES, 3 mM DPC, 20 mM rimantadine, pH 6.5. ITC sample cell contains: 25 mM MES, 3 mM DPC, pH 6.5. The volume for the first injection is 0.2 μl, the rest is 2 μl each.

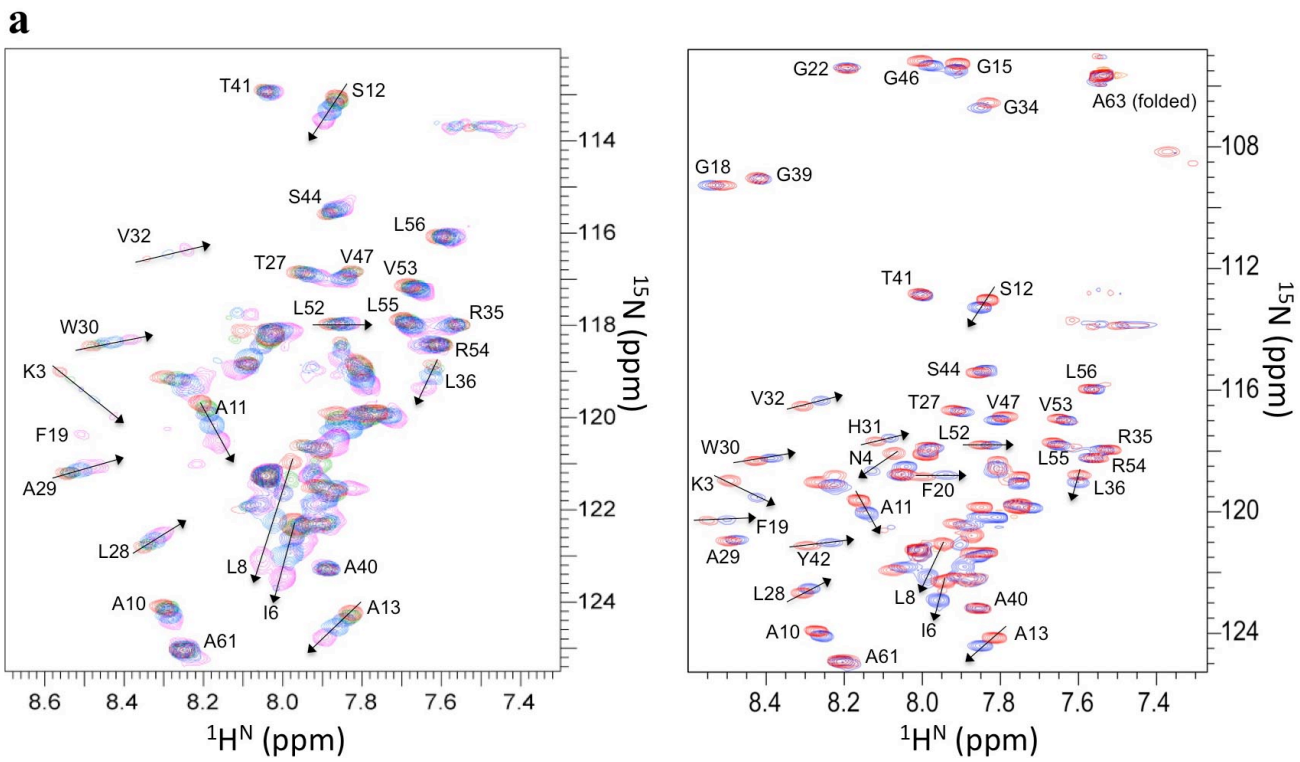
a
T41
S12
S44
V32
L56
T27
V47
V53
L52
L55
R35
W30
R54
K3
L36
A11
F19
A29
L28
L8
A40
A10
I6
A13
A61
114
116
118
120
122
124
15N (ppm)
8.6
8.4
8.2
8.0
7.8
7.6
7.4
1HN (ppm)
G22
G46
G15
G34
A63 (folded)
G18
G39
108
112
116
120
124
15N (ppm)
T41
S12
S44
L56
V32
T27
V47
V53
H31
L52
R35
W30
N4
L55
R54
K3
F20
L36
A11
F19
A29
Y42
L28
L8
A40
A10
I6
A13
A61
8.4
8.2
8.0
7.8
7.6
7.4
1HN (ppm)

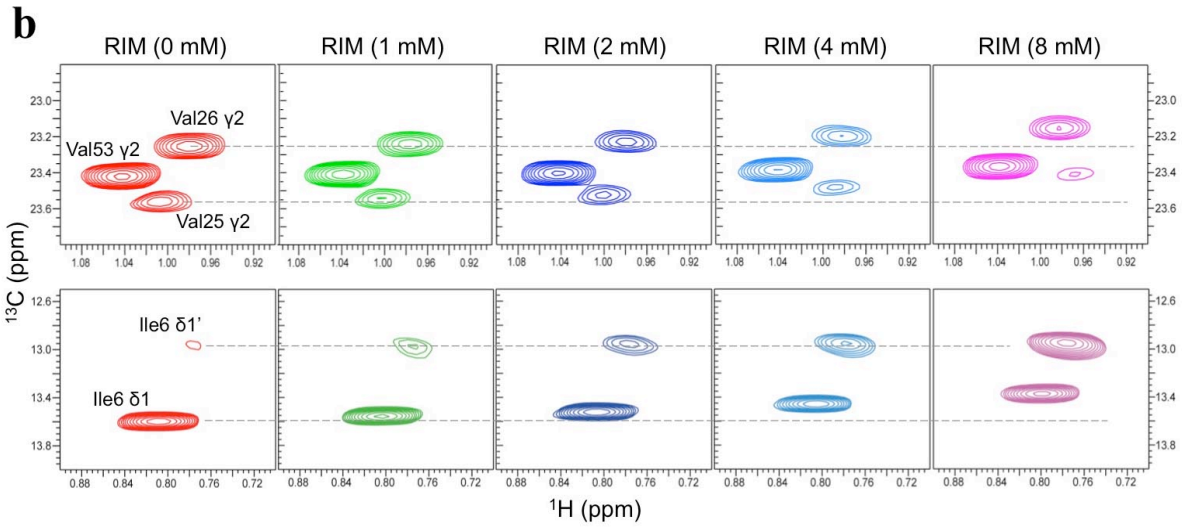
b
RIM (0 mM)
RIM (1 mM)
RIM (2 mM)
RIM (4 mM)
RIM (8 mM)
Val26 γ2
Val53 γ2
Val25 γ2
Ile6 δ1'
Ile6 δ1
13C (ppm)
1H (ppm)

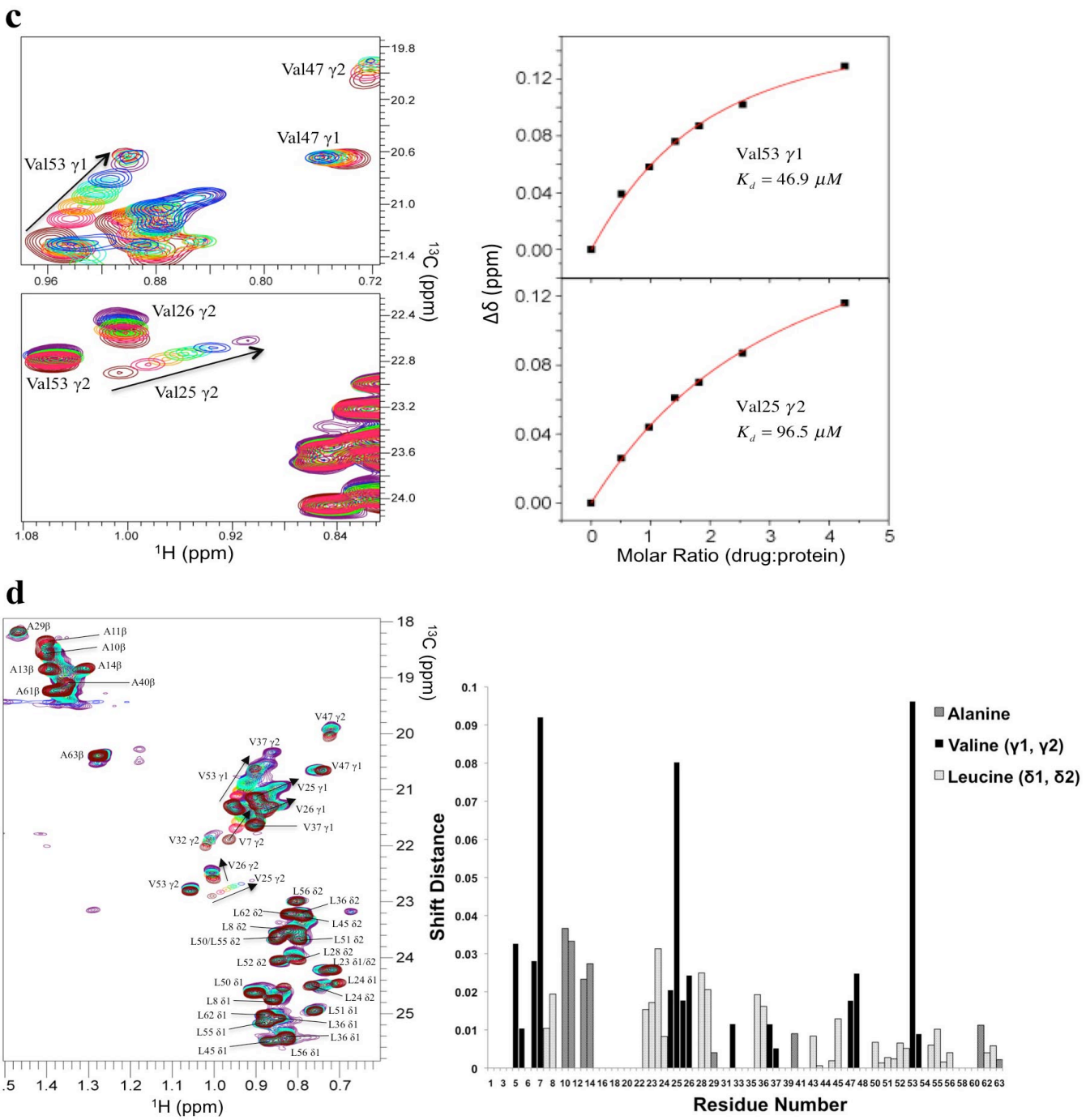

Supplementary Figure 5. Rimantadine binding significantly perturbed the chemical shifts of the p7(5a) oligomer.

a, Rimantadine titration using ^{1}H-^{15}N TROSY-HSQC as readout. **Left panel:** Uniformly (^{15}N/^{13}C)-labeled p7(5a) (monomer concentration at 0.25 mM) reconstituted in 80 mM DPC was titrated with 0 (red), 1 (green), 2 (blue), 4 (light blue), and 8 mM (pink) rimantadine. Spectra were recorded on a 750 MHz spectrometer. The resolved peaks are labeled with assignments and the arrows indicate the

movement of peaks. **Right panel:** Overlay of the TROSY-HSQC spectra of ($^{15}N/^{2}H$)-labeled p7(5a) (monomer concentration at 0.5 mM) reconstituted in 150 mM DPC in the absence of drug (red) and in the presence of 5 mM rimantadine (blue). Spectra were recorded on a 900 MHz spectrometer. The same chemical shift changes were observed for 10 mM amantadine.

b, The same samples in (**a, left panel**) above were used to record ^{13}C-HSQC spectra on a 750 MHz spectrometer. Shown in the boxes are gamma methyl resonances of valines 25, 26, and 53 (upper panel) and delta methyl resonances of Ile6. Since there is only one isoleucine in the protein, the weak peak (labeled Ile6 δ1') in the drug-free spectrum is from a minor population of the protein. Note that in the titration experiments, the effective drug concentration for protein binding can be very different from what was added to the solution due to the presence of a large amount of detergent (see Supplementary Methods for discussion).

c, Rimantadine titration at very low protein and detergent concentration. **Left panel:** Overlay of two regions of the ^{1}H-^{13}C HSQC spectra (non constant-time ^{13}C evolution) recorded at different rimantadine concentrations showing specific shifting of Val25 γ2 and Val53 γ1 methyl resonances. In this titration, the sample contains 38 μM p7 (monomer) and 3 mM DPC. The p7 is (^{1}H-/^{13}C)-labeled at the methyl positions of alanines, valines and leucines but is otherwise (^{2}H-/^{12}C) labeled. The drug stock solution is the same as in the ITC experiments. The titration protocol involved addition of 0, 10, 20, 30, 40, 60, and 120 μL drug stock solution to 250 μL protein solution. **Right panel:** Plots of chemical shift change vs. rimantadine concentration for Val25 γ2 and Val53 γ1 methyl resonances. The chemical shift change, Δδ, is defined as $\Delta\delta = [(\Delta\delta_H)^2 + (w_C\Delta\delta_C)^2]^{1/2}$, where the weighing factor, w_C, was calculated for a given atom type and amino acid based on the ratio of standard deviations of the chemical shifts stored in BioMagResBank[11,12]. Fitting of titration data to standard equilibrium binding equation (after performing the same drug concentration adjustment as in the ITC experiments) yielded apparent K_d of 96.5 and 46.9 μM for Val25 γ2 and Val53 γ1 methyl groups, respectively.

d, A more complete analysis of the rimantadine titration data in **c**. **Left panel:** Overlay of the complete methyl regions of the ^{1}H-^{13}C HSQC spectra recorded at different rimantadine concentrations. **Right panel:** Plot of chemical shift change between the first and the last titration points as a function of residue number. Since titration was performed using the ALV labeled protein, the shift changes are shown for only alanines, leucines, and valines of which the methyl resonances are sufficiently resolved for the analysis.

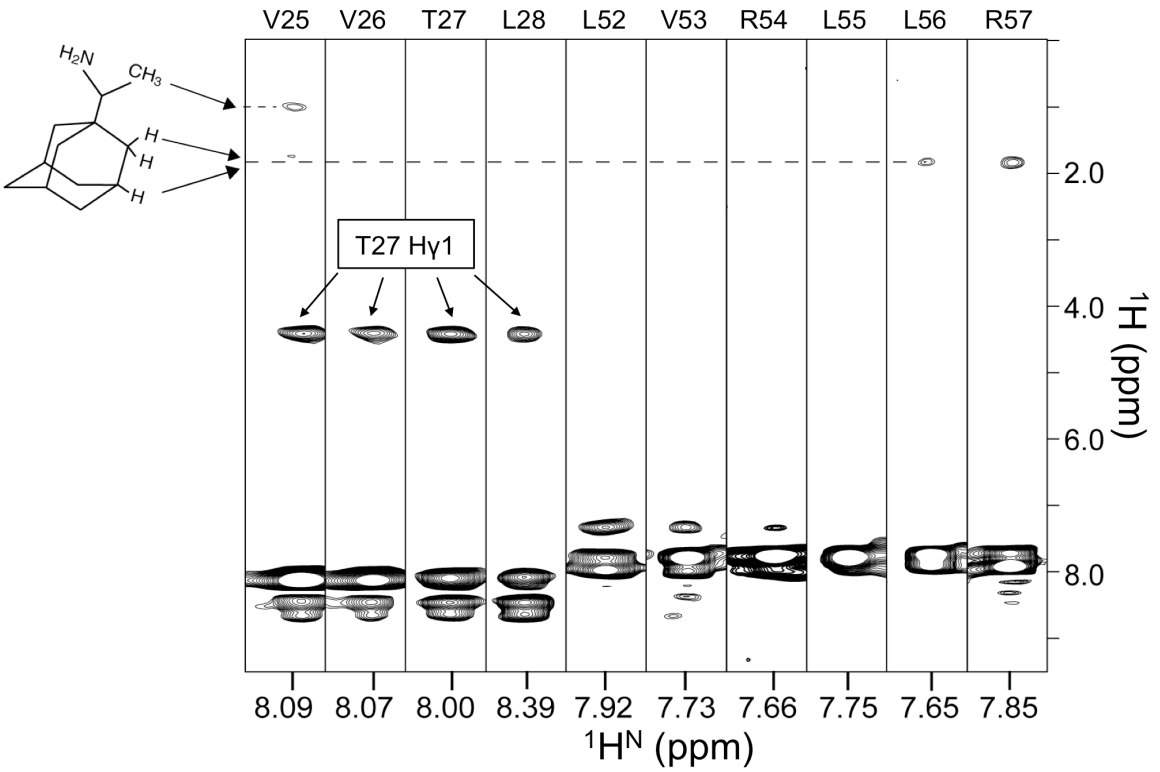

Supplementary Figure 6. Rimantadine binds to the same site in p7(5a) as amantadine. The representative strips are taken from the 3D ^{15}N-edited NOESY-TROSY (NOE mixing time of 300 ms) spectrum that was recorded at ^{1}H frequency of 750 MHz and 30 °C using a sample containing ^{15}N-, ^{2}H-labeled protein and 5 mM rimantadine (pH 6.5). The crosspeaks from 1-2 ppm are NOEs between the backbone amide protons of the p7(5a) hexamer and the protons of rimantadine.

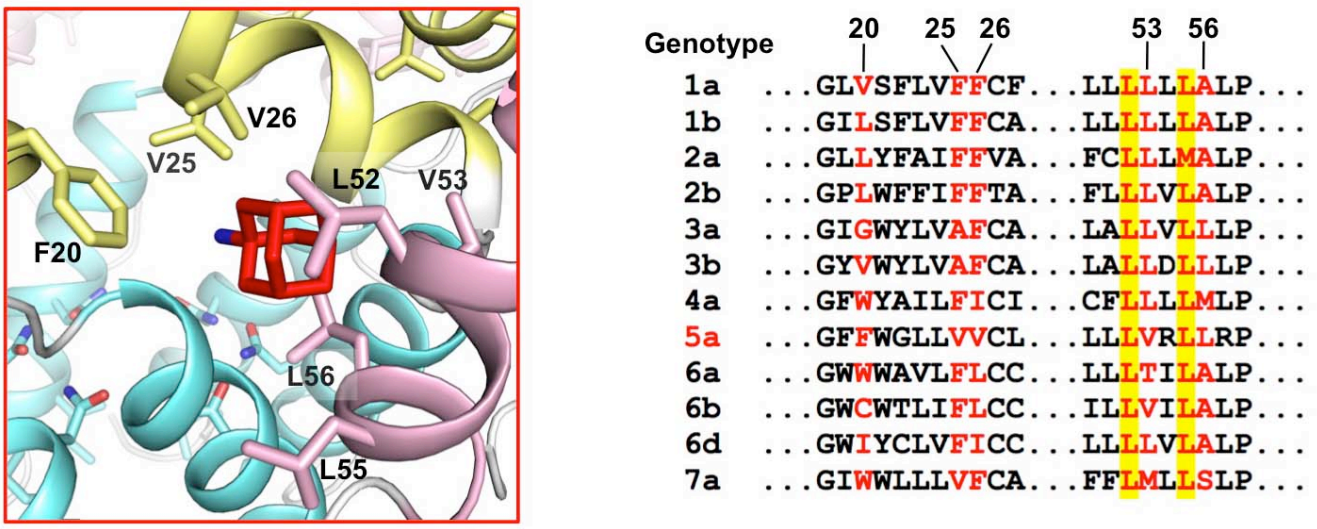

Supplementary Figure 7. Sequence alignment of the key residues in the amantadine or rimantadine binding site. The left panel shows the structure of the drug binding site. The right panel shows the alignment of drug pocket residues of p7 variants from the seven HCV genotypes. Residues in red are involved in forming the drug-binding pocket. Residues in yellow shade, Leu52 and Leu55, are highly conserved. In addition, residue positions 26 and 53 are occupied mostly by hydrophobic amino acids.

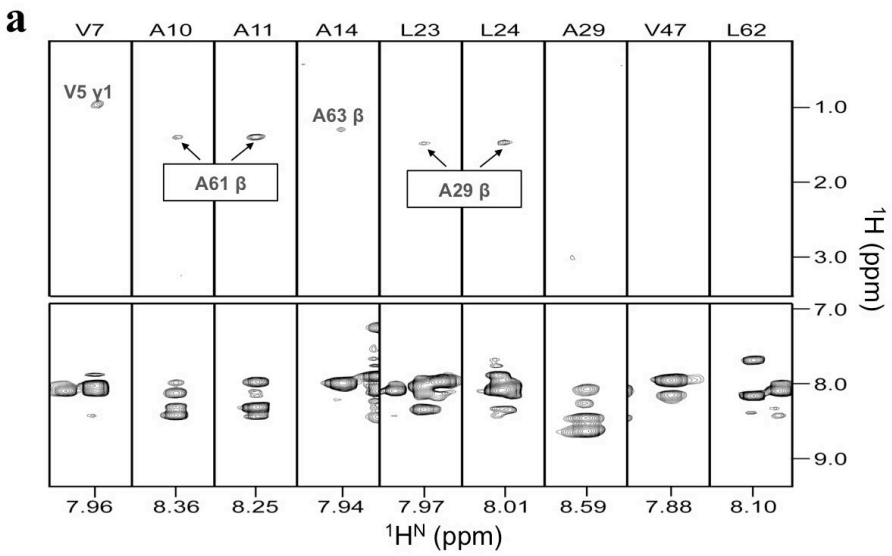
a
V7
A10
A11
A14
L23
L24
A29
V47
L62
V5 γ1
A63 β
A61 β
A29 β
1.0
2.0
3.0
7.0
8.0
9.0
^{1}H (ppm)
7.96
8.36
8.25
7.94
7.97
8.01
8.59
7.88
8.10
^{1}H^N (ppm)

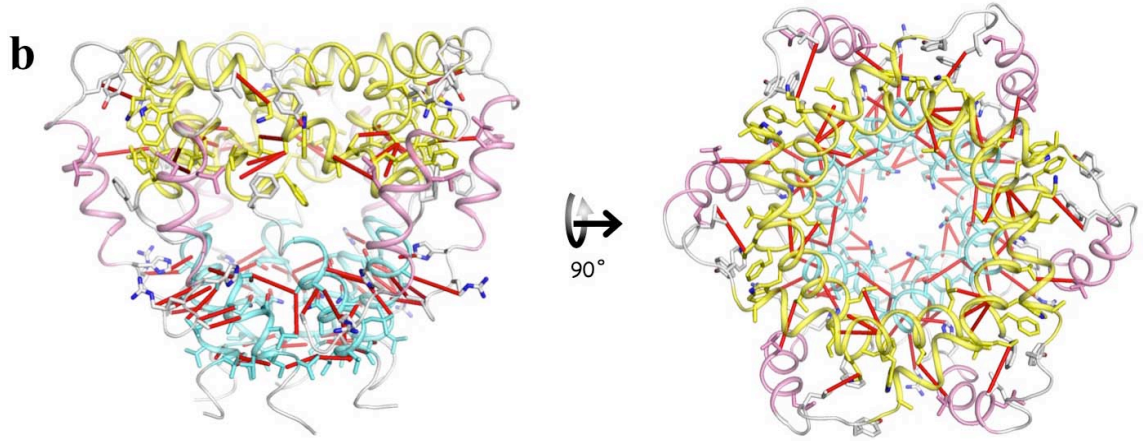
b
90°

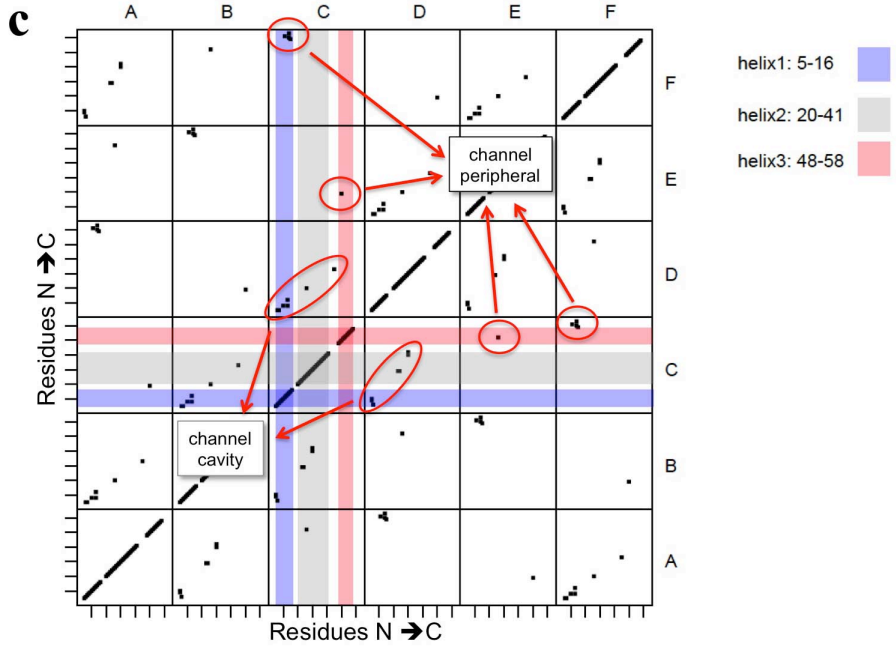
c
A
B
C
D
E
F
channel peripheral
channel cavity
Residues N →C
Residues N →C
helix1: 5-16
helix2: 20-41
helix3: 48-58

Supplementary Figure 8. Analysis of intermonomer NOEs in the p7(5b) hexamer.

a, The use of mixed isotope-labeled monomers allowed for the assignment of intermonomer NOEs. The representative strips are taken from the 3D ^{15}N-edited NOESY-TROSY (NOE mixing time of 300 ms) spectrum that was recorded at ^{1}H frequency of 900 MHz and 30 °C using a sample containing 50% ^{15}N-, ^{2}H-labeled protein and 50% uniformly ^{13}C-labeled protein (pH 6.5). The crosspeaks in the aliphatic regions are intermonomer NOEs between the backbone amide and the sidechain methyl protons.

b, Sideview and overview of the hexamer structure showing all intermonomer NOE-derived distance restraints (red lines) used in structure determination.

c, A matrix representation for showing intermonomer NOE restraints in more details. Each of the six diagonal boxes represents a monomer sequence. All 24 × 6 distance restraints are plotted in the matrix.

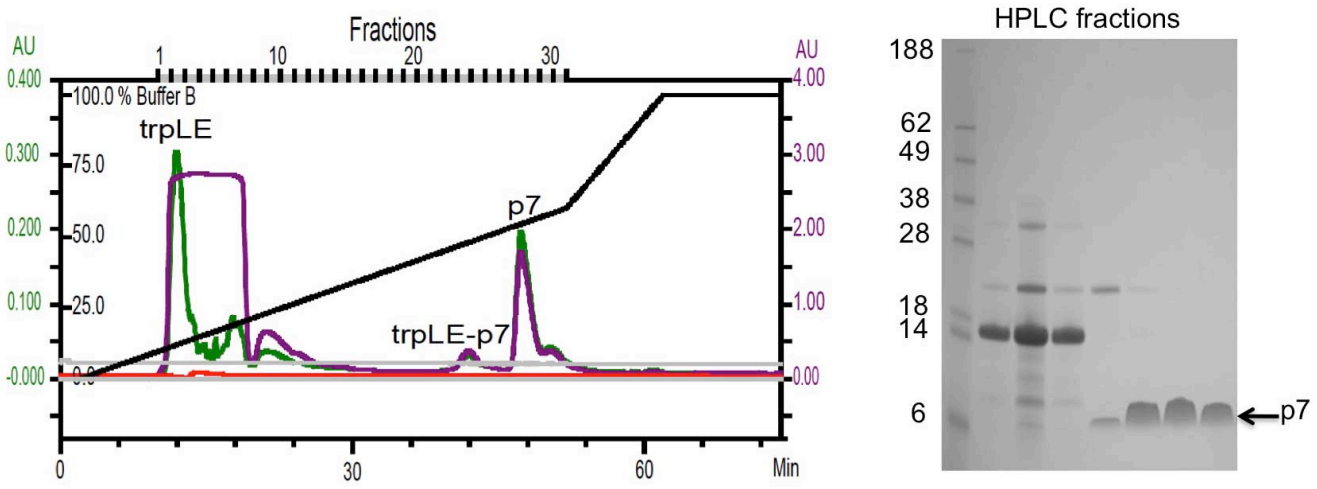

Supplementary Figure 9. HPLC purification of p7(5a) peptide. After CNBr digestion, sample was a mixture of trpLE, p7(5a), trpLE-p7(5a) fusion protein, and some other products from non-specific degradation. The p7(5a) was purified from this mixture by HPLC using a C18 column. **Left panel**: HPLC elution profile after applying a shallow gradient from 100% Buffer A (40% acetonitrile, 0.1% trifluoroacetic acid (TFA)) to 40% Buffer A and 60% Buffer B (60% acetonitrile, 0.1% TFA). **Right panel**: SDS-PAGE of the elution fractions showing the purity of the p7(5a) fractions in the last two lanes on the right.

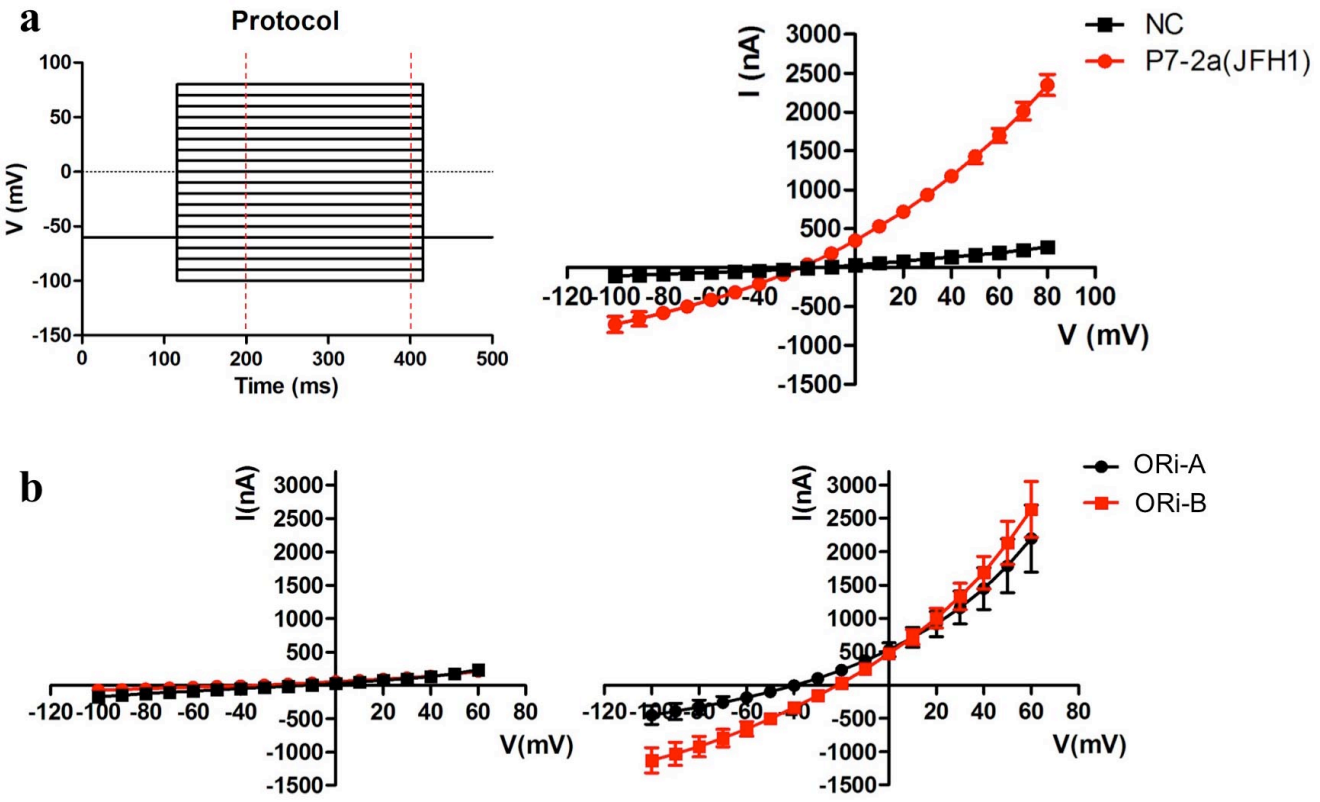

Supplementary Figure 10. Characterization of p7(2a)-mediated current across ooctye plasma membrane.

a, Injection of p7(2a) cRNA induced distinct current in oocytes. Left panel shows the standard protocol used in the two-electrode voltage-clamp recording. Right panel compares the current-voltage relationship of oocyte injected with p7(2a) cRNA to that of oocyte injected with water (NC). Each point represents the steady-state current (average current between 200-400 ms) at the corresponding voltage step. Data are presented as mean ± SEM (n=12).

b, p7(2a)-mediated current is sensitive to K^+ concentration in the ORi solution. ORi-A: 90 mM NaCl, 2 mM KCl, 2 mM $CaCl_2$, and 5 mM MOPS, pH 7.4. ORi-B: 2 mM NaCl, 100 mM KCl, 2 mM $CaCl_2$, and 5 mM MOPS, pH 7.4. Current recordings of the water-injected oocyte are shown in the left panel and that of the p7(2a)-cRNA-injected oocyte shown in the right panel. Data are presented as mean ± SEM (n=3).

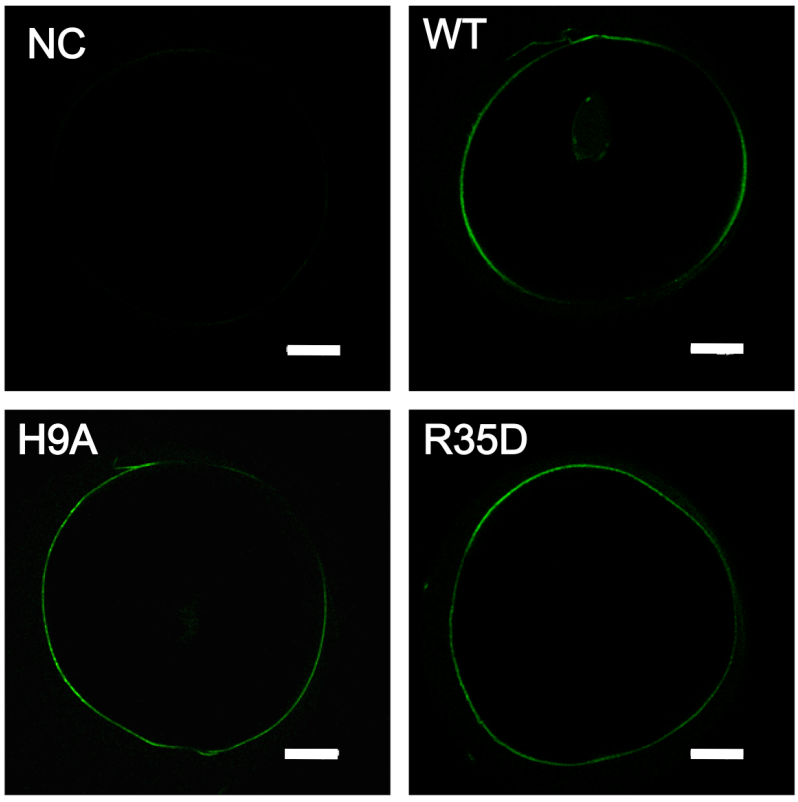

Supplementary Figure 11. Confocal microscopy of oocytes immuno-labeled with anti-HA antibody, showing that HA-tagged p7(2a) and its mutants are expressed and localized in the plasma membrane of the oocytes. The images were taken using a TCS SP2 confocal microscope. The white bar represents 200 μm in length. To quantity total amount of protein expression in the plasma membrane, we used the image analyzing software ImageJ developed by NIH (http://rsbweb.nih.gov/ij/). In this analysis, we selected pixels that cover the plasma membrane region in ImageJ. The program then plotted histogram of color intensities and calculated the total intensity in terms of grayscale values (WT: 151094; H9A: 122608; R35D: 163777).

Supplementary References

1 Mihm, U. *et al.* Amino acid variations in hepatitis C virus p7 and sensitivity to antiviral combination therapy with amantadine in chronic hepatitis C. *Antivir Ther* **11**, 507-519 (2006).

2 Foster, T. L. *et al.* Resistance mutations define specific antiviral effects for inhibitors of the hepatitis C virus p7 ion channel. *Hepatology* **54**, 79-90 (2011).

3 Wang, J. F., Schnell, J. R. & Chou, J. J. Amantadine partition and localization in phospholipids membrane: a solution NMR study. *Biochem. Biophys. Research Comm.* **324**, 212-217 (2004).

4 Tang, G. *et al.* EMAN2: an extensible image processing suite for electron microscopy. *J Struct Biol* **157**, 38-46 (2007).

5 Prodromou, C. & Pearl, L. H. Recursive PCR: a novel technique for total gene synthesis. *Protein Eng* **5**, 827-829 (1992).

6 Lu, W. *et al.* Severe acute respiratory syndrome-associated coronavirus 3a protein forms an ion channel and modulates virus release. *Proc Natl Acad Sci U S A* **103**, 12540-12545 (2006).

7 Xie, S. *et al.* DIDS blocks a chloride-dependent current that is mediated by the 2B protein of enterovirus 71. *Cell Res* **21**, 1271-1275 (2011).

8 Montserret, R. *et al.* NMR structure and ion channel activity of the p7 protein from hepatitis C virus. *J Biol Chem* **285**, 31446-31461 (2010).

9 Premkumar, A., Wilson, L., Ewart, G. D. & Gage, P. W. Cation-selective ion channels formed by p7 of hepatitis C virus are blocked by hexamethylene amiloride. *FEBS Lett* **557**, 99-103 (2004).

10 Luik, P. *et al.* The 3-dimensional structure of a hepatitis C virus p7 ion channel by electron microscopy. *Proc Natl Acad Sci U S A* **106**, 12712-12716 (2009).

11 Mulder, F. A., Schipper, D., Bott, R. & Boelens, R. Altered flexibility in the substrate-binding site of related native and engineered high-alkaline Bacillus subtilisins. *J Mol Biol* **292**, 111-123 (1999).

12 Schumann, F. H. *et al.* Combined chemical shift changes and amino acid specific chemical shift mapping of protein-protein interactions. *J Biomol NMR* **39**, 275-289 (2007).